R. & M. No. 3419

MINISTRY OF AVIATION

AERONAUTICAL RESEARCH COUNCIL
REPORTS AND MEMORANDA

Measurements of the Direct Pitching-Moment Derivatives for Three Wing Planforms at High Subsonic Speeds

By J. B. BRATT, B.A., B.Sc., W. G. RAYMER, B.Sc.(Eng.)
and J. E. G. TOWNSEND
OF THE AERODYNAMICS DIVISION, N.P.L.

LONDON: HER MAJESTY'S STATIONERY OFFICE
1965
PRICE 13*s.* 6*d.* NET

Measurements of the Direct Pitching-Moment Derivatives for Three Wing Planforms at High Subsonic Speeds

By J. B. BRATT, B.A., B.Sc., W. G. RAYMER, B.Sc.(Eng.)
and J. E. G. TOWNSEND
OF THE AERODYNAMICS DIVISION, N.P.L.

*Reports and Memoranda No. 3419**
November, 1953

Summary.

Measurements of the direct pitching damping and stiffness derivatives for a delta and two swept wing planforms made in the N.P.L. 9½ in. High Speed Tunnel are discussed, and results for the delta are compared with theory.

Experiments to investigate the cause of loss of damping at low frequencies obtained in earlier tests are also described, and the effect on derivative measurements of random oscillatory flow disturbances is examined.

LIST OF CONTENTS

* Replaces A.R.C. 16 267.

Published with the permission of the Director, National Physical Laboratory.

---

1. *Introduction.*

The measurements of the direct pitching-moment derivatives m_θ and $m_{\dot{\theta}}$ described in this paper were made in the N.P.L. $9\frac{1}{2}$ in. High Speed Tunnel using apparatus originally designed for two-dimensional work[1], but in this case adapted for three-dimensional tests. The planforms tested were a delta (Wing A) and two swept wings (Wings B and C).

Earlier measurements on these planforms made in the same wind tunnel with the same equipment had shown a rapid loss of damping at the higher Mach numbers for values of the frequency parameter below 0·3 to 0·4 and the smaller amplitudes of oscillation. This led to negative damping at the smallest amplitudes, and sustained or growing oscillations were obtained. With Wing C, negative damping was obtained at Mach numbers as low as 0·4 with an amplitude of 1 degree.

Considerable doubt was felt as to whether this effect could be a true characteristic of the planforms which would occur in free flight, or whether it arose from local conditions, and a number of tests were made using Wing C in an attempt to establish a cause. This investigation led to the discovery of random oscillatory disturbances to the flow in the tunnel working section resulting from a badly designed tunnel intake. An account of this investigation is given below and is followed by a discussion of the derivative measurements obtained after modification to the tunnel intake. Curves showing the earlier results are included in Figs. 5 to 32 for comparison.

2. *Details of Models.*

The models were constructed of solid steel, and each represented half of a complete wing without body. They are illustrated to full scale in Figs. 2, 3 and 4. The data below relate to a complete wing.

	Wing A	Wing B	Wing C
Apex angle	90°	60°	92·46°
Sweepback (L.E.)	45°	60°	43·77°
Sweepback (T.E.)	0°	52°	25·74°
Aspect ratio	3·00	2·88	4·42
Taper ratio	0·143	—	0·311
Root chord	4·000 in.	3·630 in.	3·453 in.

	Wing A	Wing B	Wing C
Tip chord	0·572 in.	—	1·074 in.
Mean chord	2·286 in.	2·356 in.	2·264 in.
Span	6·856 in.	6·786 (ignoring tip radius)	10·000 in.
Thickness/chord ratio	10%	6% to 7%	10%
Section	RAE 102	—	EQ 1040
Axis positions (distance behind apex)	$0·556c_0$ $0·431c_0$	$0·799c_0$ $0·689c_0$	$0·809c_0$ $0·722c_0$
A.C. position (distance behind apex)	$0·534c_0$ (low speed)	0·865 (low speed) 0·901 ($M = 0·9$)	$0·792c_0$ ($M = 0·70$)

3. *Tests on Loss of Damping for Low ω.*

3.1. *Tunnel Boundary Layer.*

In the half-wing technique employed with the derivative apparatus used on the $9\frac{1}{2}$ in. tunnel the root of the model is immersed in the boundary layer on one of the walls of the tunnel. In comparison with two-dimensional models, for which the apparatus was originally designed, a larger percentage of the area of finite-aspect-ratio models of the type under consideration will be affected by the tunnel boundary layer. Since no loss of damping had been observed in two-dimensional tests at low values of ω, it was thought that the greater influence of the tunnel boundary layer might be the cause of the loss in the finite-aspect-ratio tests.

To test this suggestion a false wall was constructed spanning the tunnel working section and displaced $\frac{1}{2}$ in. from the tunnel wall. The model was displaced an equal amount towards the centre of the tunnel. With this arrangement the thickness of the boundary layer affecting the model was reduced considerably, but tests could not be carried out for Mach numbers greater than 0·6 on account of a deterioration in the velocity distribution.

Measurements were made with Wing C at nominal Mach numbers of 0·4 with a frequency of 11·1 c/s and 0·4, 0·5, 0·6 with a frequency of 23·3 c/s. The results agreed reasonably well with those obtained without the false wall and showed that the tunnel boundary layer had little affect.

3.2. *Model Boundary Layer.*

The maximum Reynolds number reached in the $9\frac{1}{2}$ in. tunnel is approximately 1×10^6, and for this low value the model boundary layer is mainly laminar. A suggestion that laminar separations arising during oscillation might be the cause of the loss of damping under investigation was examined by making the model boundary layer turbulent. This was accomplished by means of transition wires fixed at 0·1 c from the leading edge, the change from laminar to turbulent flow being checked by the 'oil film' technique.

Measurements were made with the turbulent boundary layer at nominal Mach numbers of 0·4 and 0·7, and frequencies of 11·1 and 23·3 c/s. These results differed little from those obtained with the laminar boundary layer.

3.3. *Fluctuations in Flow Direction.*

At this point in the investigation attention was directed to the possibility of some periodic disturbance in the tunnel flow affecting the measurements of damping. A static calibration preceding the derivative measurements had shown a reasonably uniform velocity distribution, but nothing was known about oscillatory disturbances.

A qualitative test was first made by traversing the empty tunnel with a silk thread attached to a probe. This indicated some disturbance at the centre of the working section, and quantitative measurements were then obtained at this position with a hot-wire yawmeter arranged to measure the instantaneous direction in a plane parallel to the wind stream and perpendicular to the model. From general considerations this was thought to be the type of disturbance most likely to affect measurements involving pitching oscillations. The output from the yawmeter was observed with a cathode-ray oscilloscope and indicated a fluctuation in flow direction with time which at $M = 0{\cdot}4$ attained a maximum value of approximately $\pm 7\frac{1}{2}$ degrees from the mean direction. Tests at higher Mach numbers were unsuccessful due to the fine wires forming the yawmeter breaking under the drag load.

Attempts were made to determine a definite periodic component of the fluctuation, first by means of a tuneable inductance-capacity filter and later with a wattmeter harmonic analyser. The results of both tests were negative, however, the fluctuation appearing to be completely random.

An investigation into the cause of these fluctuations led to the discovery of large disturbances in the tunnel intake. These were observed with a tuft of wool on a probe, and appeared to result mainly from a separation at the floor of the tunnel which gave rise to large eddies and considerable swirl. The original form of the tunnel intake is shown diagrammatically in Fig. 1a. The tunnel is vertical, and air enters the intake through six gauzes symmetrically disposed about the tunnel axis. No provision had been made to guide the air into the flare, and a dead-air region formed at the centre of the tunnel floor.

Tests were made with a 100-mesh gauze across the entrance to the flare, but this had no measurable effect on the fluctuations in the working section.

In order to improve the entry conditions a specially shaped cone was constructed and fixed to the tunnel floor as indicated in Fig. 1b. The cone was formed by six curved surfaces which guided the flow from each of the entry gauzes into the vertical direction. A set of six rectangular plates radiated from the axis of the cone at angular positions which corresponded to the junctions of the surfaces and formed a system of straighteners for removing any remaining tendency to swirl.

Tests made with the hot-wire yawmeter after fitting the cone showed a very marked improvement in the steadiness of the flow in the working section, the maximum fluctuation in direction at $M = 0{\cdot}4$ now amounting to $\pm \frac{1}{2}$ degree as compared with $\pm 7\frac{1}{2}$ degrees obtained previously. With the unsteady flow conditions Wing C when free to pitch about the $0{\cdot}722c_0$ axis at the lowest test frequency (12 c/s), had oscillated spontaneously with an amplitude of 1 degree at $M = 0{\cdot}4$. With the improved flow conditions this amplitude was reduced to 1/8th degree. Measurements of the pitching damping now showed no falling off at low values of the frequency parameter for amplitudes of 1 and 2 degrees. Measurements at small amplitudes were regarded as unreliable since the free-oscillation test mentioned above had indicated complete loss of damping on approaching an amplitude of 1/8th degree. In fact it appears that in oscillatory work a lower limit to the test amplitude exists below which oscillatory fluctuations in flow direction can have a large effect on the measurements at low values of the frequency parameter and the higher wind speeds. It appears also from subsequent tests that the effect depends largely on planform and is not present with unswept models.

4. *Tests with Improved Flow Conditions.*

In view of the very unsatisfactory flow conditions which were present during the earlier tests on the three models, it was thought desirable to repeat a large number of the measurements, and amended curves are given in the present report. Curves for the 'bad flow' condition are also included for comparison.

The measurements were repeated for amplitudes of 1 degree and 2 degrees and a mean incidence of 0 degrees for all the three models. Tests were also made for mean incidences of 3 degrees and 5 degrees with Wing A.

For each model two axis positions were used, one behind and the other ahead of the aerodynamic centre (A.C.) in the case of Wings A and C. This was not possible with Wing B, both axes being ahead of the A.C. for structural reasons.

Measurements of $-m_{\dot{\theta}}$ and $-m_{\theta}$ are shown in Figs. 5 to 32 as functions of Mach number for still-air frequencies ranging from 11 to 57 c/s nominal, the Mach number range being from 0·4 to 0·95 approximately. Curves showing the variation of the frequency parameter ω with Mach number for each frequency are also included. The frequency parameter ranged from 0·015 to 0·16 approximately.

Figures 33 to 48 are derived from the earlier figures by cross-plotting to show the variation of $-m_{\dot{\theta}}$ and $-m_{\theta}$ with ω for given values of M, whilst Figs. 49 to 51 show the variation with M for a fixed frequency parameter $\omega = 0{\cdot}07$.

4.1. *Effects at Low ω.*

It is clear from the figures that, with the improved flow, the loss of damping at low values of the frequency parameter and small amplitude of oscillation has been eliminated for Wing C with the forward axis position and very much reduced with the rearward position. In the case of Wing A the loss has been considerably reduced for both axes at a mean incidence of 0 degrees, whilst in the tests at incidence the frequency parameter did not extend to a low enough value to show any effect if present. In the case of Wing B the loss of damping at low ω appears to be very little altered by the improvement in the flow, but this model had exhibited the effect to a smaller extent than the others for the amplitudes of the test.

4.2. *Additional Effects.*

Apart from the effects at low ω the improvement in the steadiness of the flow has had a considerable influence on some of the curves in general. The most marked effect is the introduction in some cases of a large amplitude effect on the damping, which goes in the opposite direction from that associated with unsteady flow and low values of ω. The smaller amplitude now corresponds to the greater damping. This effect is present to a marked degree for the forward axis positions in the tests on the swept wings but is absent with the delta, which seems to suggest that it is associated with a swept trailing edge. Corresponding amplitude effects appear in the curves of aerodynamic stiffness, the smaller amplitude corresponding to the smaller stiffness.

A further effect occurs at the high Mach number end of some of the curves of damping and stiffness plotted against Mach number. In the case of Wing C with the rearward axis position, what was previously a loss of damping above $M = 0{\cdot}87$ becomes a continual rise, whilst with the delta at incidence a previous rise becomes a fall above $M = 0{\cdot}9$. The stiffness curves for Wing C with the rearward axis and for the delta at 0 degrees incidence with both axes now indicate a rapid forward movement of the aerodynamic centre above $M = 0{\cdot}9$.

These features have been mentioned in order to emphasize the misleading results which can be obtained in some cases in oscillation work when flow unsteadiness of the type described is present. As far as is known no unusual features had been observed in earlier static work carried out in the same tunnel. This is not surprising, however, since such tests would have been made with two-dimensional unswept models, and oscillation tests made subsequently to those described in the present report have shown that with a two-dimensional model the presence of the cone in the tunnel intake to improve the flow has little effect on the results.

5. *Further Tests on Wing B.*

In view of the large amplitude effect on the amended damping curves for Wing B with the forward axis position it was thought desirable to make some measurements with an extended amplitude range in this case. These additional tests were carried out with slotted liners fitted to the tunnel, since they were made during a series of transonic tests. An amplitude range of 1 to 4 degrees was covered for a Mach number range of 0·4 to 0·7 with a still-air frequency of 35·1 c/s. The curves of $-m_{\dot{\theta}}$ given in Fig. 54 show a rapid flattening out of amplitude effect above 2 degrees.

6. *Comparisons with Theory.*

Curves from Fig. 49 showing the variation of $-m_{\dot{\theta}}$ and $-m_{\theta}$ with M for $\omega = 0{\cdot}07$ for the delta are compared in Figs. 52 and 53 with curves based on two different theoretical treatments. One of these, due to Garner[2], is based on Multhopp's theory and was obtained by satisfying the downwash condition at seven spanwise and two chordwise positions using the amended treatment given in Appendix II of Ref. 2. The curve due to Lehrian[3] was calculated on the basis of the vortex lattice method due to W. P. Jones[4] using a 21 × 6 lattice. Both theoretical curves relate to values of the frequency parameter tending to zero, and compressibility effects were introduced by treating the equivalent planform in incompressible flow as described in Ref. 5.

The two theoretical treatments are in reasonable agreement. In comparison the experimental curves of $-m_{\dot{\theta}}$ are 25 to 30 per cent low in the middle of the Mach number range. Better agreement is obtained at the lower Mach numbers. At the highest Mach number of the range good agreement with theory is obtained in the forward axis case, whilst with the rearward axis experiment is 37 per cent low. The curves of $-m_{\theta}$ are in satisfactory agreement with theory except at the highest Mach number end, where the experimental curves indicate a rapid forward movement of the aerodynamic centre.

7. *Comparisons with R.A.E. Tests.*

Low-speed measurements of oscillatory derivatives for Wings A and C have been made in an $11\frac{1}{2}$ ft × $8\frac{1}{2}$ ft tunnel by Moss[6] at the R.A.E. Decaying oscillation and inexorable forcing techniques were used, the models being complete wings situated at the centre of the tunnel working section. Values of $-m_{\dot{\theta}}$ and $-m_{\theta}$ for $M = 0{\cdot}19$ and $\omega = 0{\cdot}1$ derived from these tests for the delta are included in Figs. 52 and 53 and show satisfactory agreement with the N.P.L. experimental curves. Values of $-m_{\dot{\theta}}$ for the swept wing for the same values of M and ω are included in Fig. 51 and show good agreement with the rearward axis curve. The value for the forward axis is about 20 per cent low compared with the extrapolated N.P.L. curve for 2 degrees amplitude. From the trend of amplitude effect in this case it seems probable that better agreement would be obtained at still higher amplitudes.

8. *Conclusions.*

The main conclusions based on the amended curves (Figs. 49 to 52) are summarized below.

8.1. *Wing A.*

(i) For both axis positions and 0 degrees incidence the damping increases by a factor of 2·5 approximately for an increase of Mach number from 0·4 to 0·95, the rate of increase of damping being greater at the higher Mach numbers.

(ii) In the tests at incidence (3 degrees and 5 degrees) the rise in damping ceases at approximately $M = 0{\cdot}9$ and is followed by a fall. The rise is much greater at 5 degrees incidence, the damping increasing by a factor of 4 approximately for a change of Mach number from 0·4 to 0·9.

(iii) The stiffness-derivative curves for 0 degrees incidence indicate a gradual rearward movement of the aerodynamic centre with increasing Mach number followed by a rapid forward movement above $M = 0{\cdot}9$. This becomes a fairly rapid rearward movement in the tests at incidence.

(iv) Comparison with R.A.E. low-speed tests is very satisfactory. Comparison with theory is satisfactory for the stiffness derivative below $M = 0{\cdot}9$. The experimental values of the damping derivative are 25 to 30 per cent low in the middle of the Mach number range, agreement improving towards the low Mach number end. Good agreement with theory is obtained for the forward axis case at $M = 0{\cdot}9$.

8.2. *Wing B.*

(i) The increase in damping with Mach number is much less than for Wing A, and for the forward axis position reaches a maximum at $M = 0{\cdot}9$, which is followed by a slight fall.

(ii) Large amplitude effects on damping are present with the forward axis position, the damping for 1 degree being 35 to 40 per cent greater than for 2 degrees. With the rearward axis the effect is reduced to 10 to 20 per cent. Tests at higher amplitudes show a rapid flattening out of this effect above 2 degrees amplitude.

(iii) The stiffness-derivative curves in this case give no indication of rapid movements of the aerodynamic centre. Amplitude effects are present as in the case of the damping, but in comparison these are somewhat smaller in magnitude and are of opposite sign, the stiffness for 1 degree being less than for 2 degrees.

8.3. *Wing C.*

(i) An increase in damping with Mach number of a similar character and order of magnitude to that obtained with Wing A is observed up to $M = 0{\cdot}92$, above which value the damping for the forward axis position begins to fall.

(ii) A large amplitude effect on damping is present with the forward axis position, the damping for 1 degree being approximately 50 per cent greater than that for 2 degrees at the higher Mach numbers.

(iii) The stiffness-derivative curves indicate a gradual rearward movement of the aerodynamic centre with increasing Mach number followed by a rapid forward movement above $M = 0{\cdot}9$ at the higher amplitude. An amplitude effect is present with the forward axis position, the stiffness for 1 degree being less than for 2 degrees. The magnitude of the effect is less than that observed with the damping.

(iv) Comparison with R.A.E. low-speed measurements of damping is satisfactory for the rearward axis position. For the forward axis the R.A.E. result is 20 per cent low compared with the extrapolated N.P.L. curve for 2 degrees amplitude.

The occurrence of amplitude effects appears to be associated with forward axis position and a swept trailing edge.

The frequency parameter ω has negligible effect on the derivatives at the lower Mach numbers (Figs. 33 to 48). At the higher Mach numbers an effect is observed in some cases but this is not of sufficient magnitude to alter the character of the variation of the derivatives with Mach number.

NOTATION

M'		Pitching moment about axis due to wind $= M_\theta\theta + M_{\dot\theta}\dot\theta$
θ		Angular displacement about axis
θ_0		Amplitude of oscillation
α		Mean incidence
m_θ	$=$	$M_\theta/\rho SV^2\bar{c}$
$m_{\dot\theta}$	$=$	$M_{\dot\theta}/\rho SV\bar{c}^2$
ρ		Density
S		Area
V		Wind speed
$\bar{c}$		Mean chord
c_0		Root chord
f		Frequency in wind
f_0		Frequency in still air
ω		Frequency parameter $= 2\pi f\bar{c}/V$
M		Mach number

REFERENCES

No.	*Author(s)*	*Title, etc.*
1	J. B. Bratt, W. G. Raymer and J. E. G. Townsend	Measurements of the direct pitching-moment derivatives for two-dimensional flow at subsonic and supersonic speeds and for a wing of aspect ratio 4 at subsonic speeds. A.R.C. R. & M. 3257. January, 1959.
2	H. C. Garner	Multhopp's subsonic lifting-surface theory of wings in slow pitching oscillations. A.R.C. R. & M. 2885. July, 1952.
3	Doris E. Lehrian	Calculation of stability derivatives for oscillating wings. A.R.C. R. & M. 2922. February, 1953.
4	W. P. Jones	The calculation of aerodynamic derivative coefficients for wings of any plan form in non-uniform motion. A.R.C. R. & M. 2470. December, 1946.
5	W. P. Jones	Oscillating wings in compressible subsonic flow. A.R.C. R. & M. 2855. October, 1951.
6	G. F. Moss	Low-speed wind tunnel measurements of longitudinal oscillatory derivatives on three planforms. A.R.C. R. & M. 3009. November, 1952.

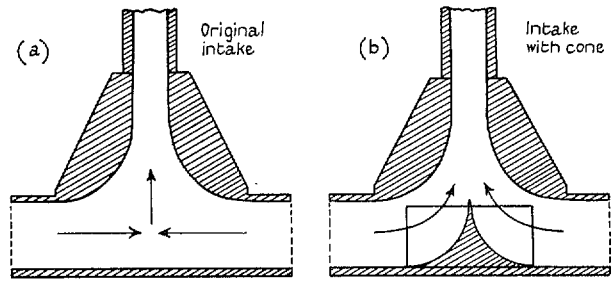

FIG. 1. Arrangement of tunnel intake.

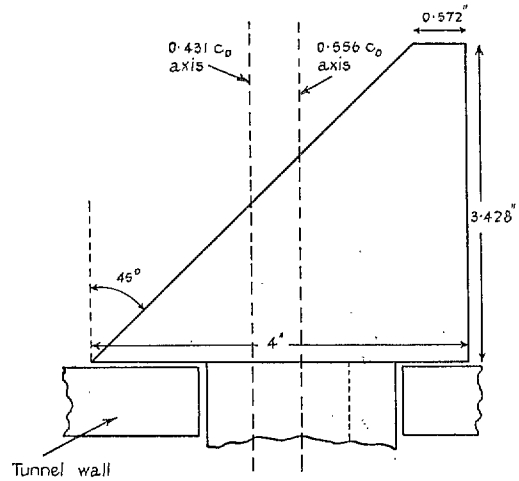

FIG. 2. Diagram of Wing A (half-scale).

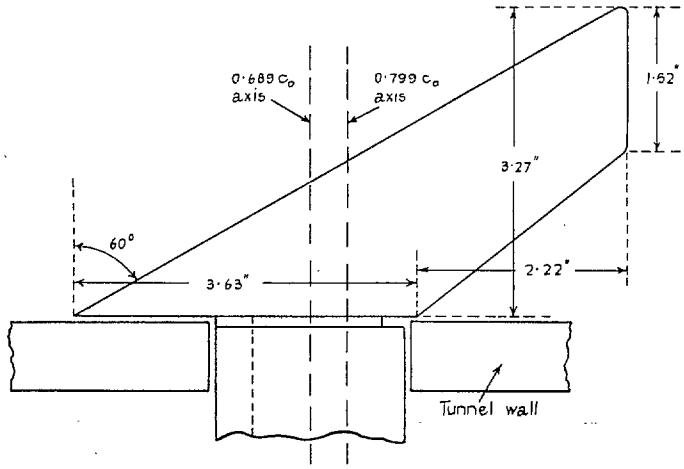

FIG. 3. Diagram of Wing B (half-scale).

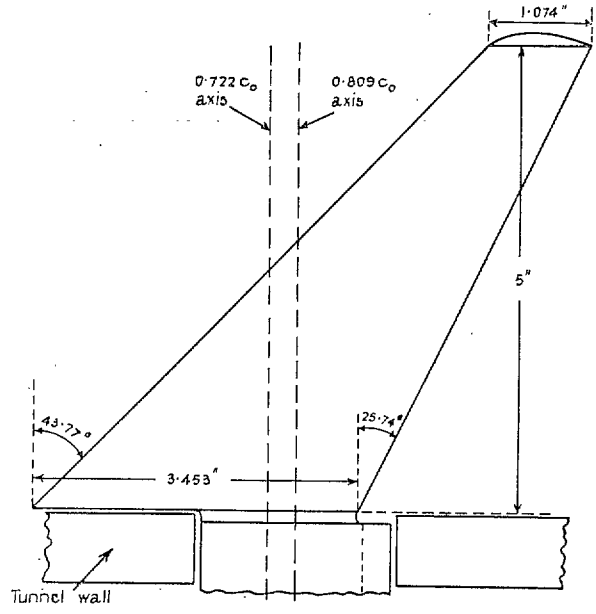

FIG. 4. Diagram of Wing C (half-scale).

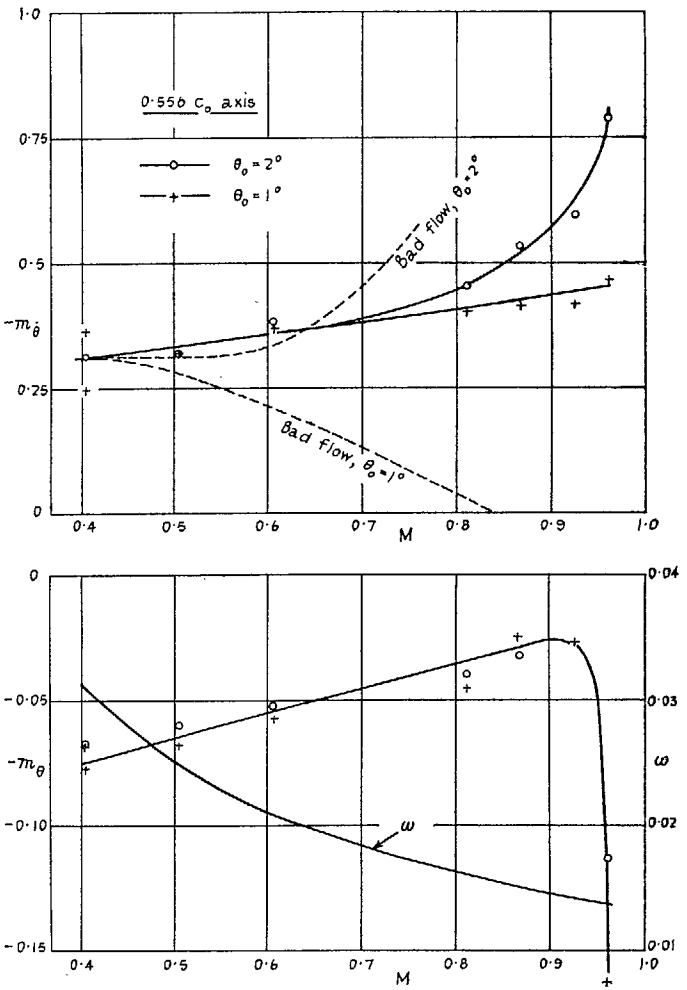

FIG. 5. Wing A—Values of $-m_{\dot\theta}$ and $-m_\theta$ for $\alpha = 0°$ and $f_0 = 11{\cdot}3$ c/s.

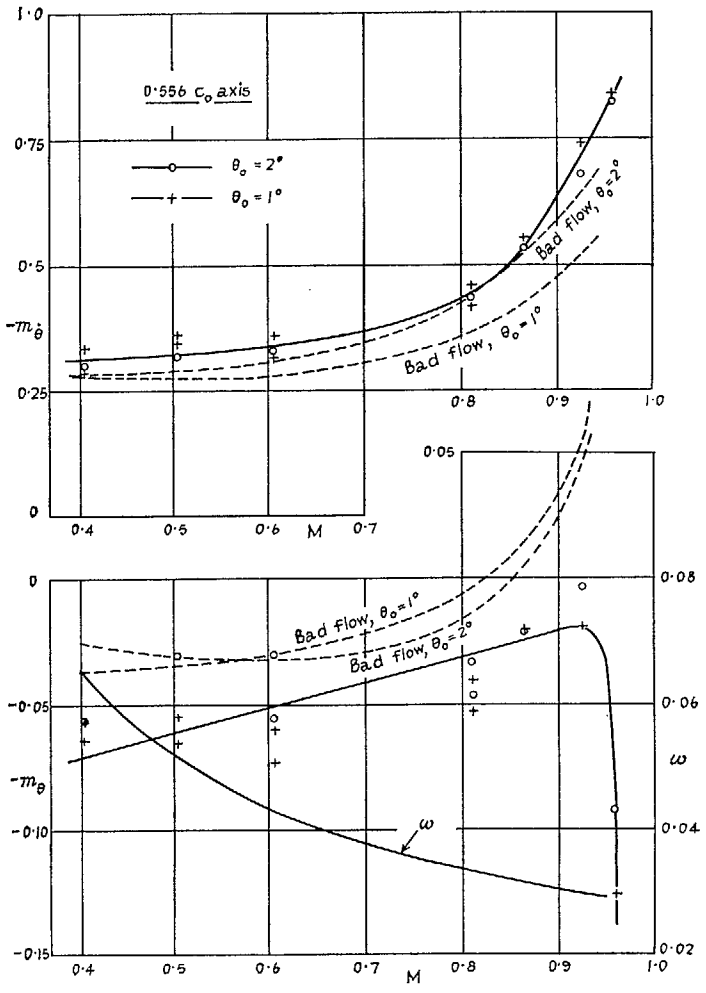

FIG. 6. Wing A—Values of $-m_{\dot\theta}$ and $-m_\theta$ for $\alpha = 0°$ and $f_0 = 23{\cdot}5$ c/s.

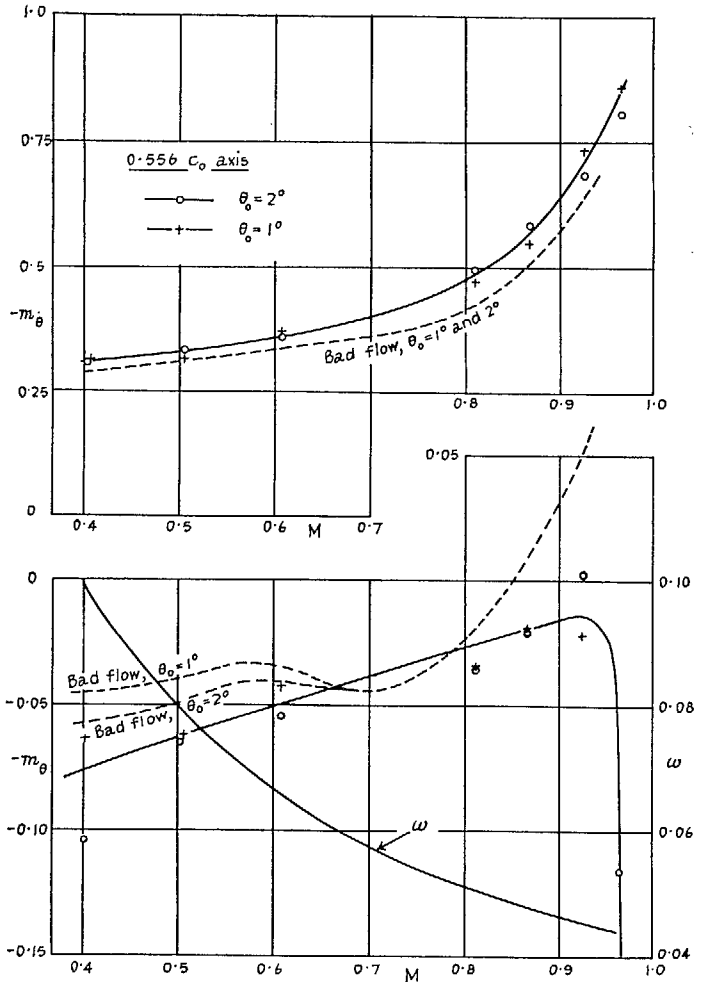

FIG. 7. Wing A—Values of $-m_{\dot\theta}$ and $-m_\theta$ for $\alpha = 0°$ and $f_0 = 35{\cdot}3$ c/s.

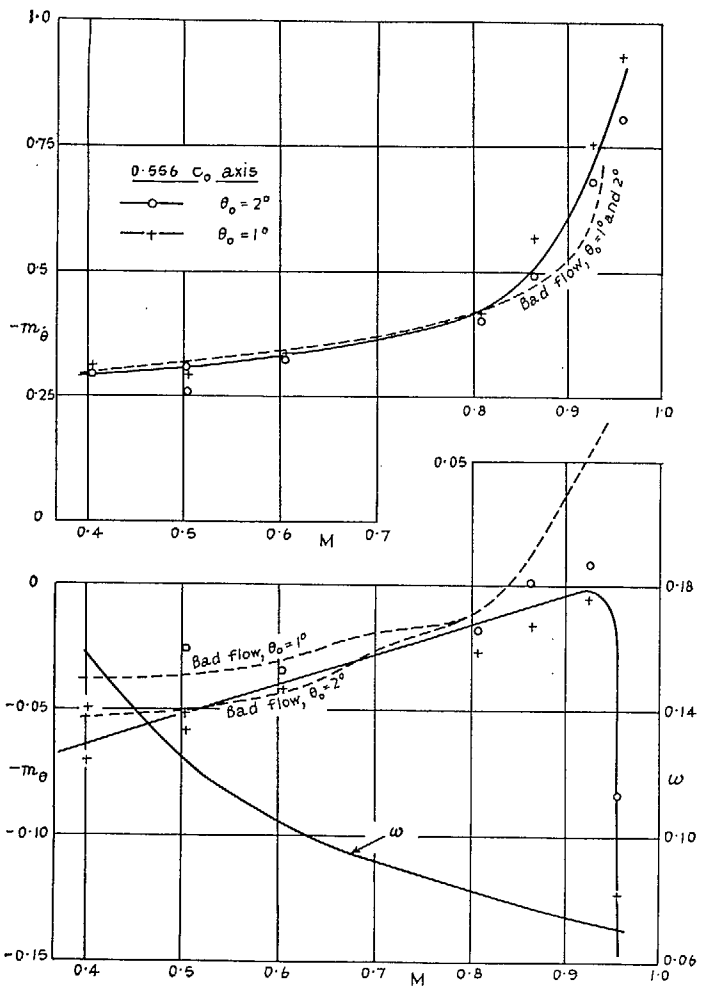

FIG. 8. Wing A—Values of $-m_{\dot\theta}$ and $-m_\theta$ for $\alpha = 0°$ and $f_0 = 57{\cdot}4$ c/s.

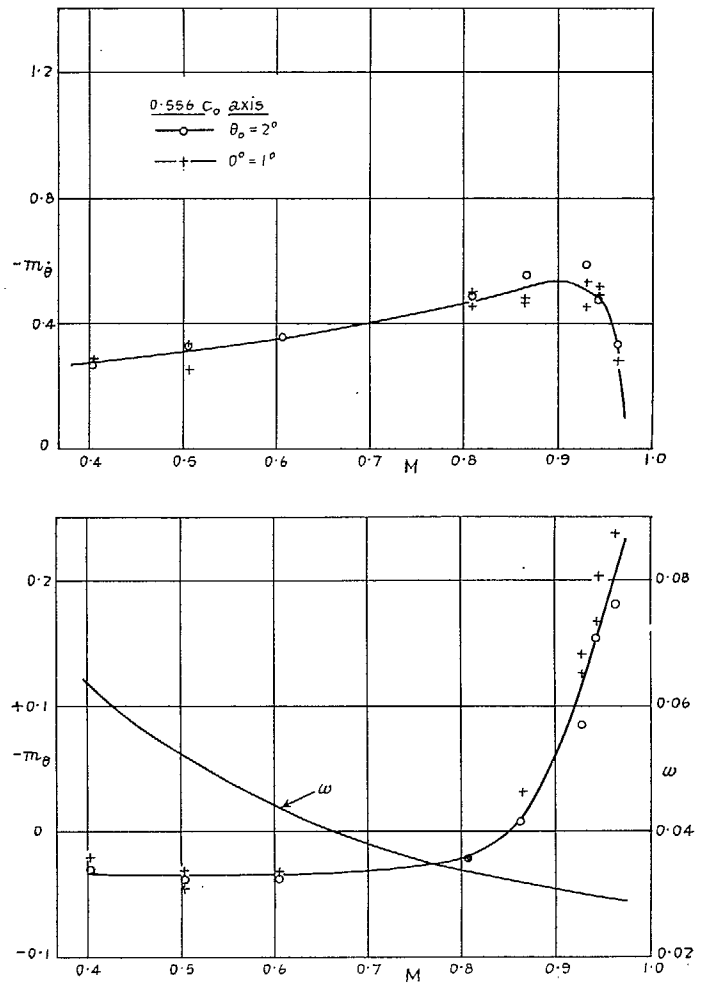

FIG. 9. Wing A—Values of $-m_{\dot\theta}$ and $-m_\theta$ for $\alpha = 3°$ and $f_0 = 23{\cdot}5$ c/s.

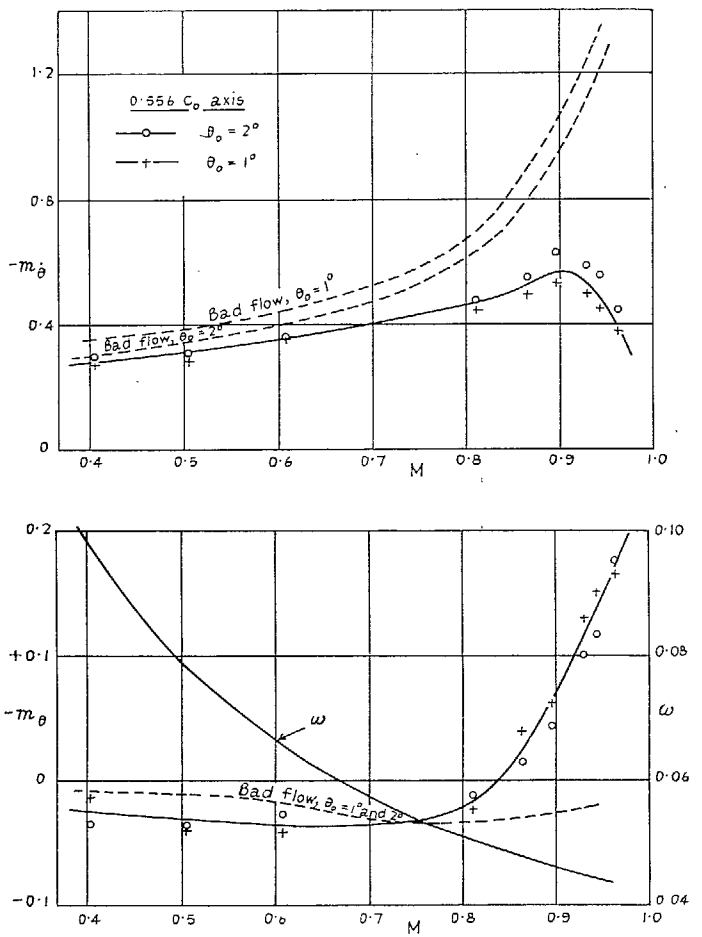

FIG. 10. Wing A—Values of $-m_{\dot\theta}$ and $-m_\theta$ for $\alpha = 3°$ and $f_0 = 35{\cdot}3$ c/s.

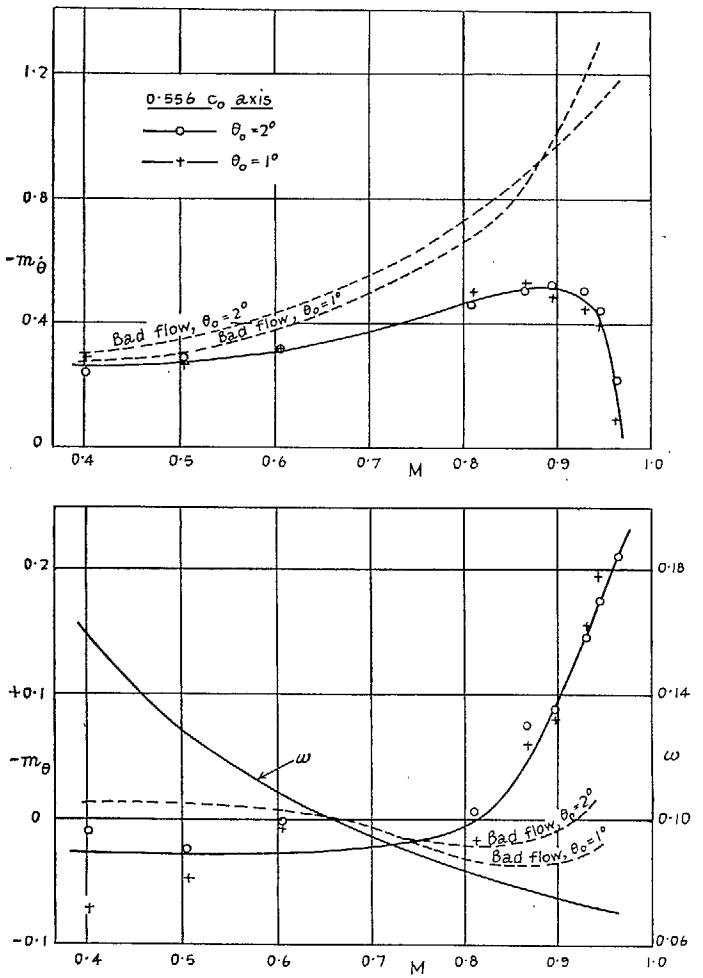

FIG. 11. Wing A—Values of $-m_{\dot\theta}$ and $-m_\theta$ for $\alpha = 3°$ and $f_0 = 57{\cdot}4$ c/s.

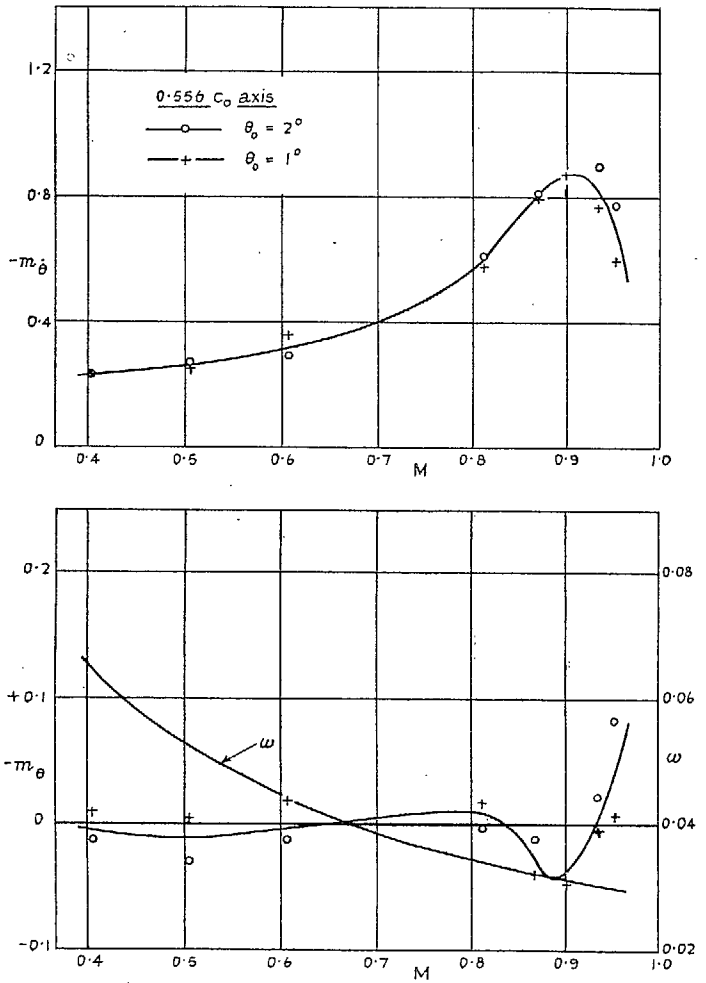

FIG. 12. Wing A—Values of $-m_{\dot\theta}$ and $-m_\theta$ for $\alpha = 5°$ and $f_0 = 23{\cdot}5$ c/s.

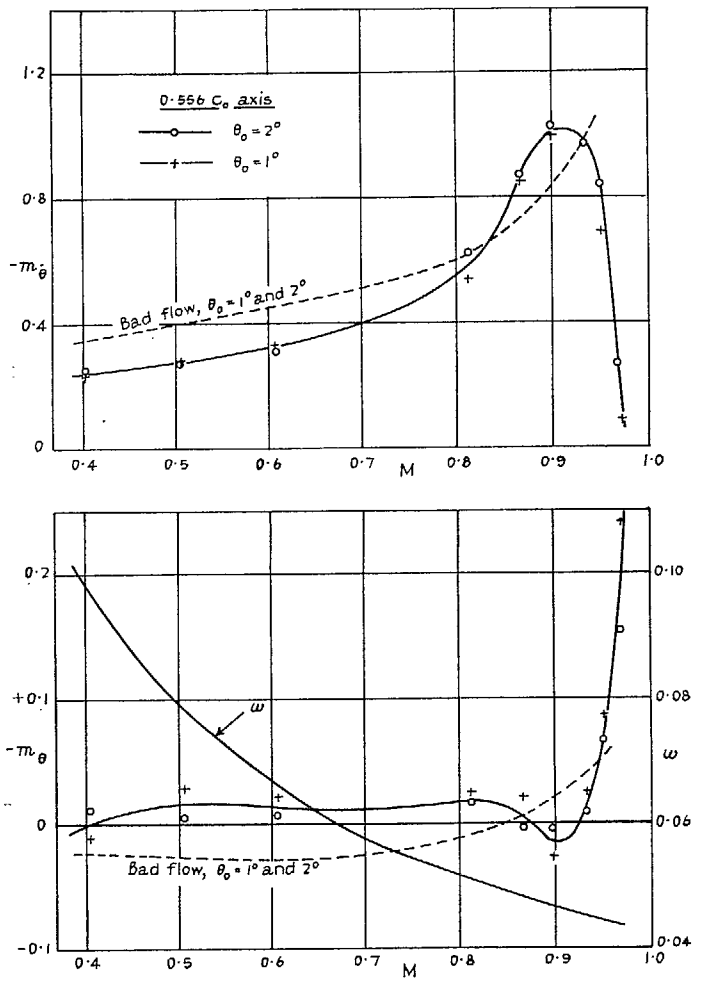

FIG. 13. Wing A—Values of $-m_{\dot\theta}$ and $-m_\theta$ for $\alpha = 5°$ and $f_0 = 35{\cdot}3$ c/s.

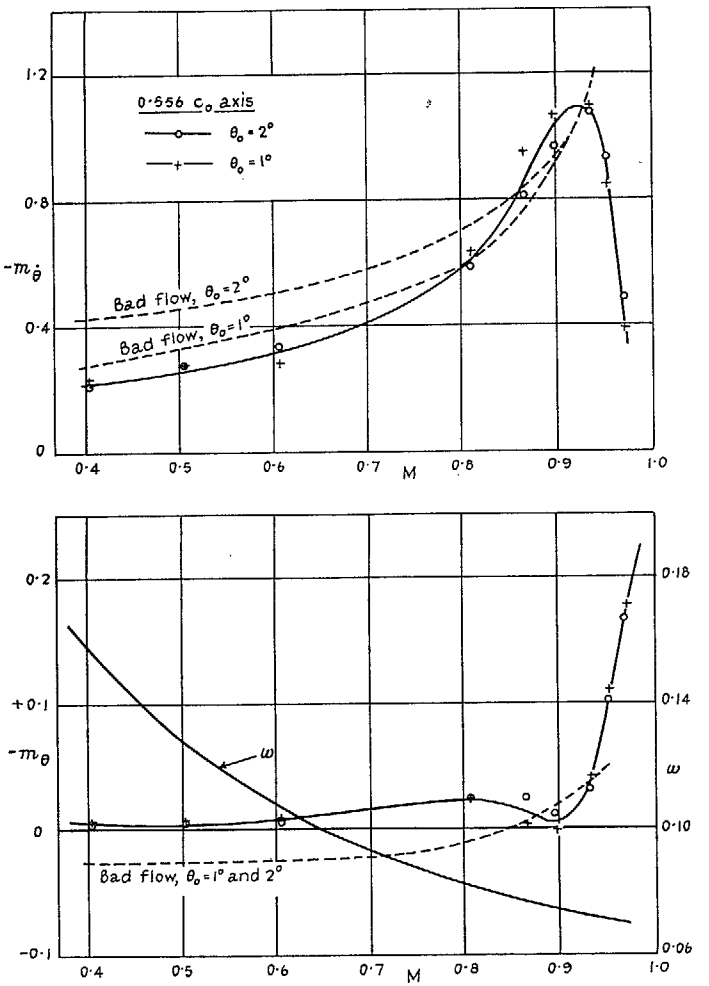

FIG. 14. Wing A—Values of $-m_{\dot\theta}$ and $-m_\theta$ for $\alpha = 5°$ and $f_0 = 57{\cdot}4$ c/s.

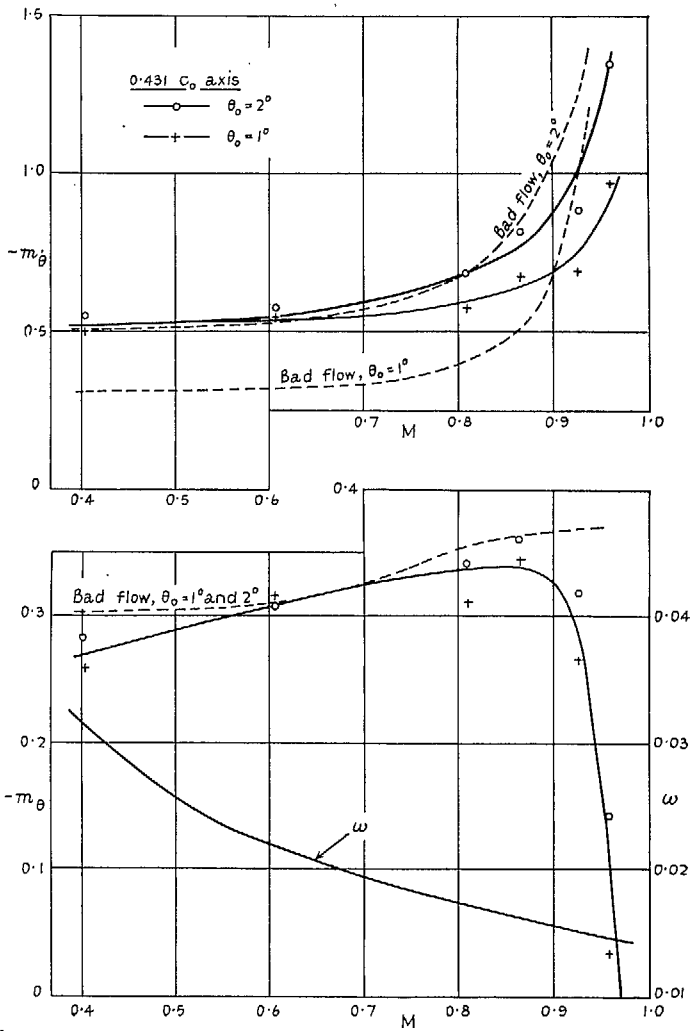

FIG. 15. Wing A—Values of $-m_{\dot\theta}$ and $-m_\theta$ for $\alpha = 0°$ and $f_0 = 11{\cdot}2$ c/s.

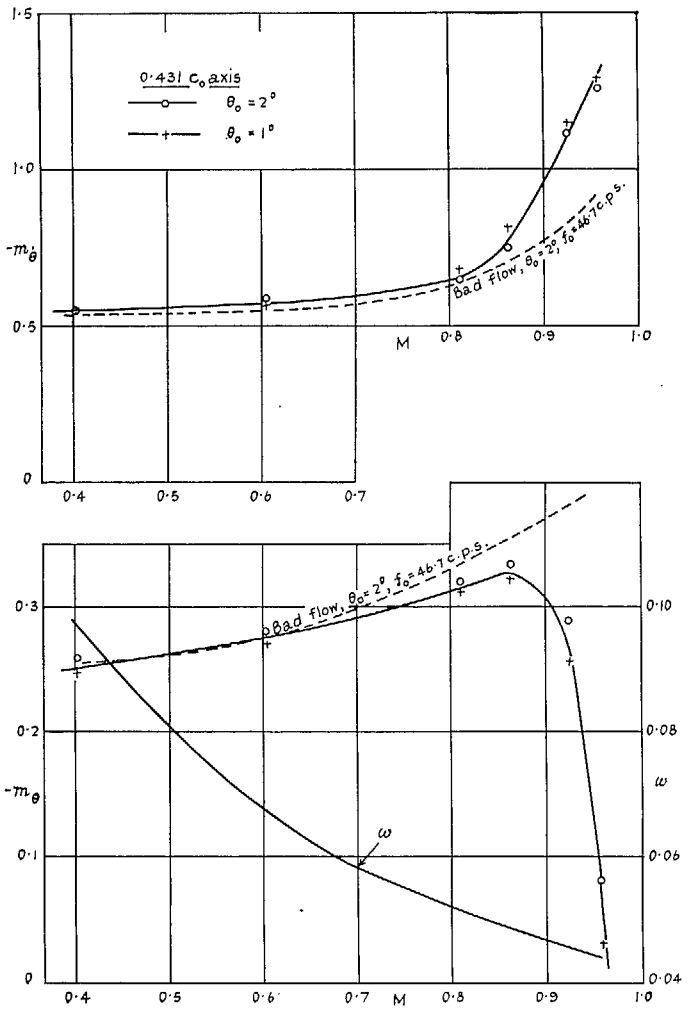

FIG. 16. Wing A—Values of $-m_{\dot\theta}$ and $-m_\theta$ for $\alpha = 0°$ and $f_0 = 35{\cdot}3$ c/s.

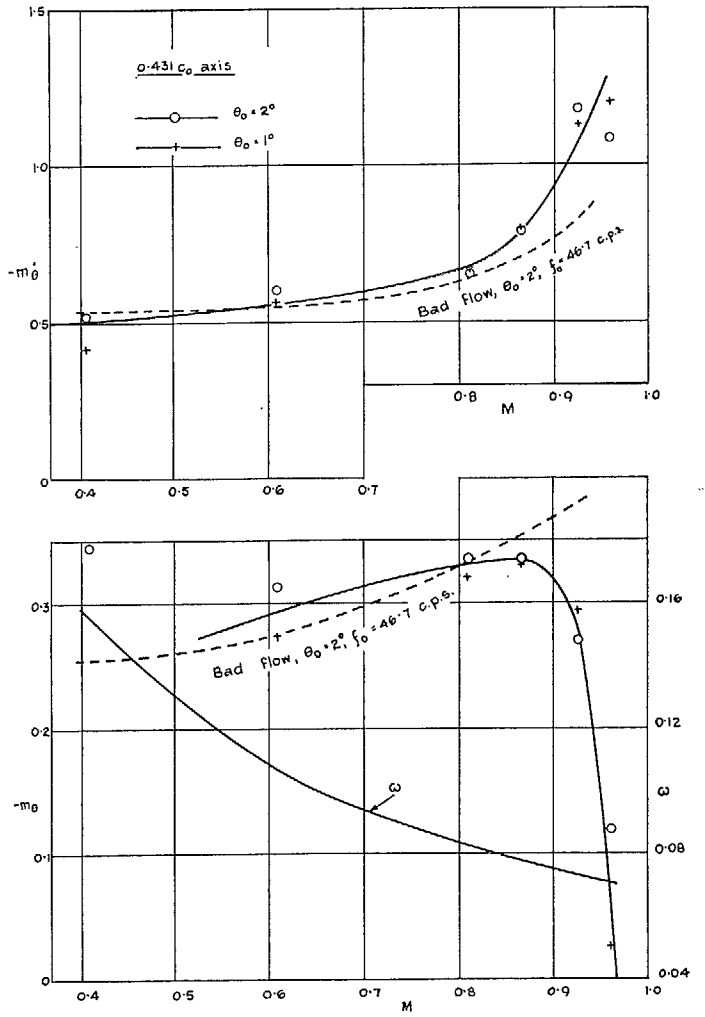

FIG. 17. Wing A—Values of $-m_{\dot\theta}$ and $-m_\theta$ for $\alpha = 0°$ and $f_0 = 57·3$ c/s.

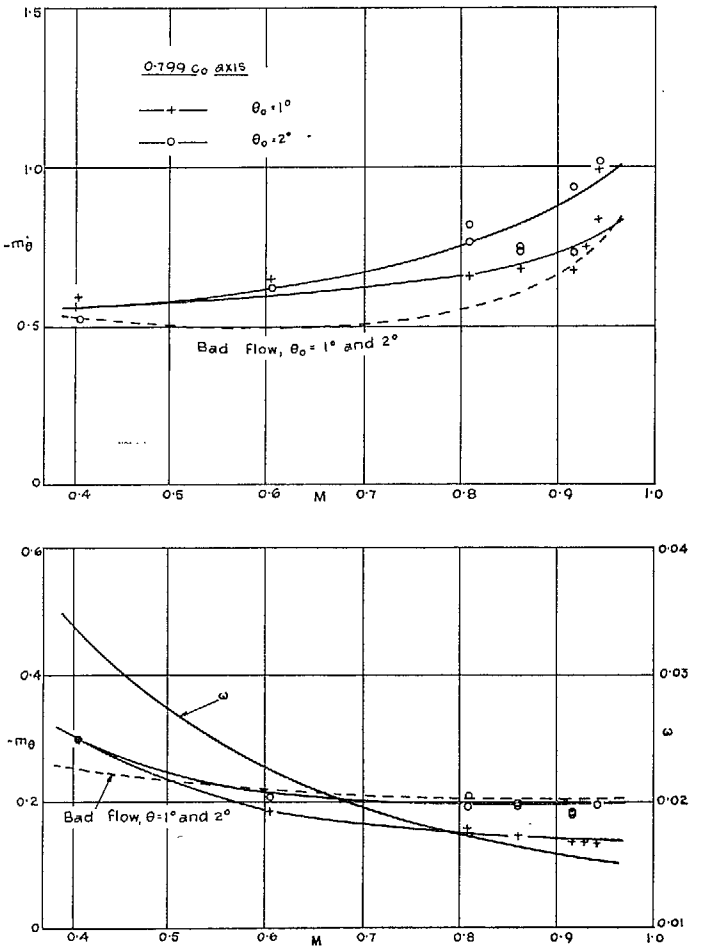

FIG. 18. Wing B—Values of $-m_{\dot\theta}$ and $-m_\theta$ for $\alpha = 0°$ and $f_0 = 11·2$ c/s.

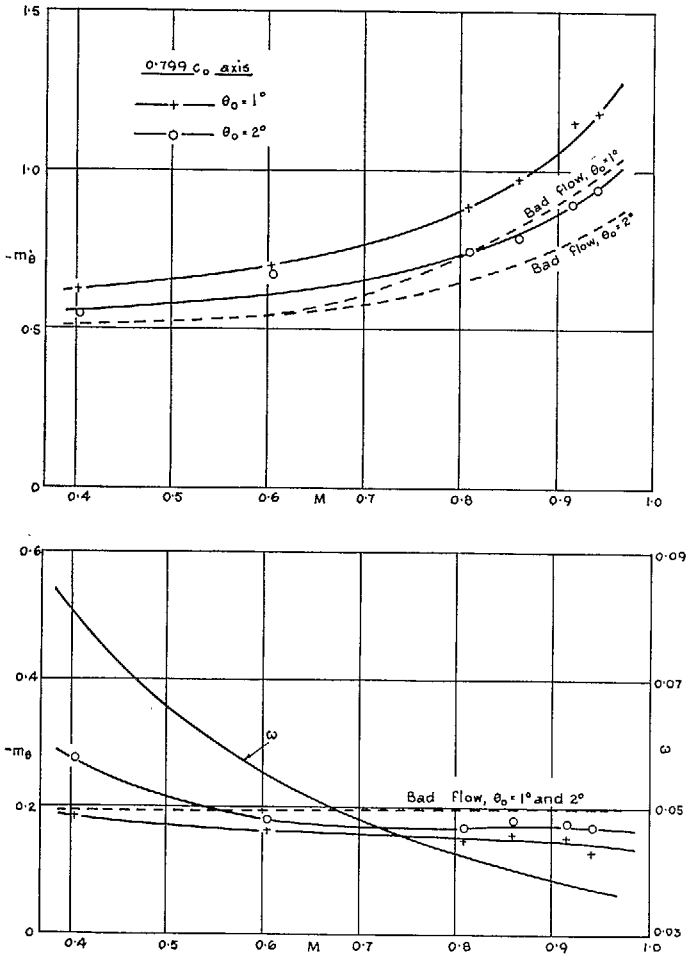

FIG. 19. Wing B—Values of $-m_{\dot\theta}$ and $-m_\theta$ for $\alpha = 0°$ and $f_0 = 35{\cdot}2$ c/s.

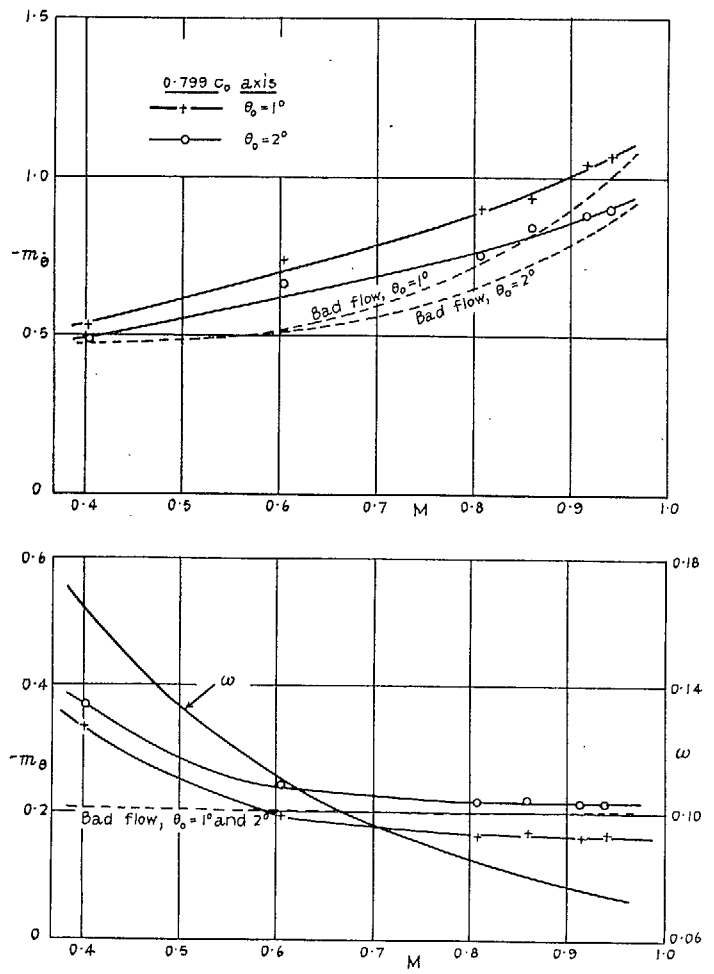

FIG. 20. Wing B—Values of $-m_{\dot\theta}$ and $-m_\theta$ for $\alpha = 0°$ and $f_0 = 57{\cdot}2$ c/s.

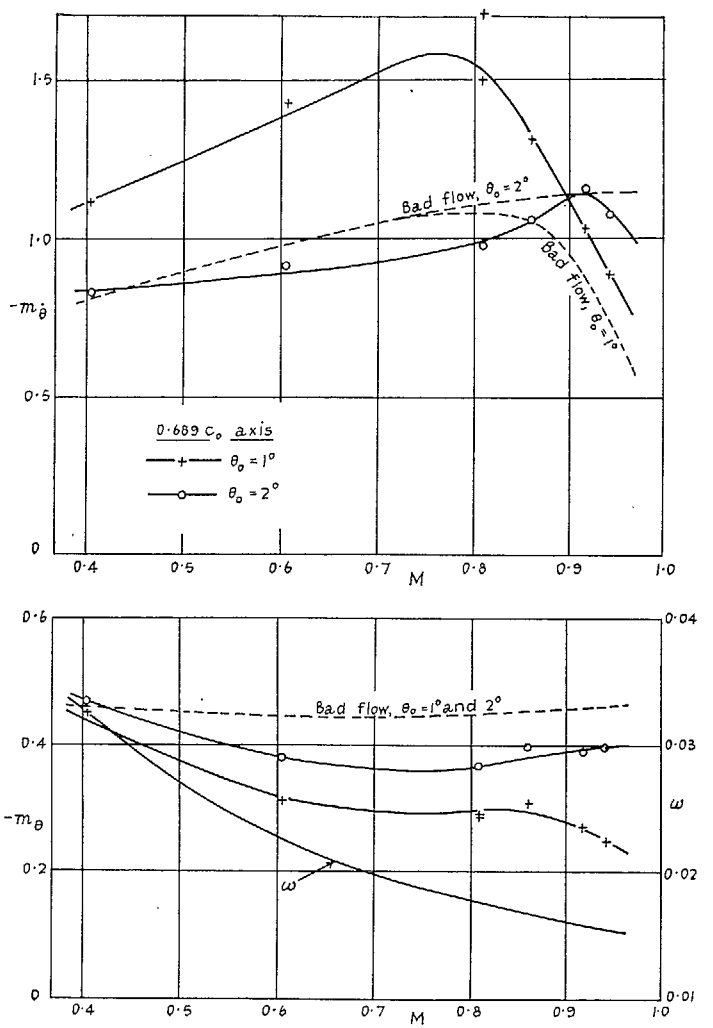

FIG. 21. Wing B—Values of $-m_{\dot{\theta}}$ and $-m_\theta$ for $\alpha = 0°$ and $f_0 = 11{\cdot}2$ c/s.

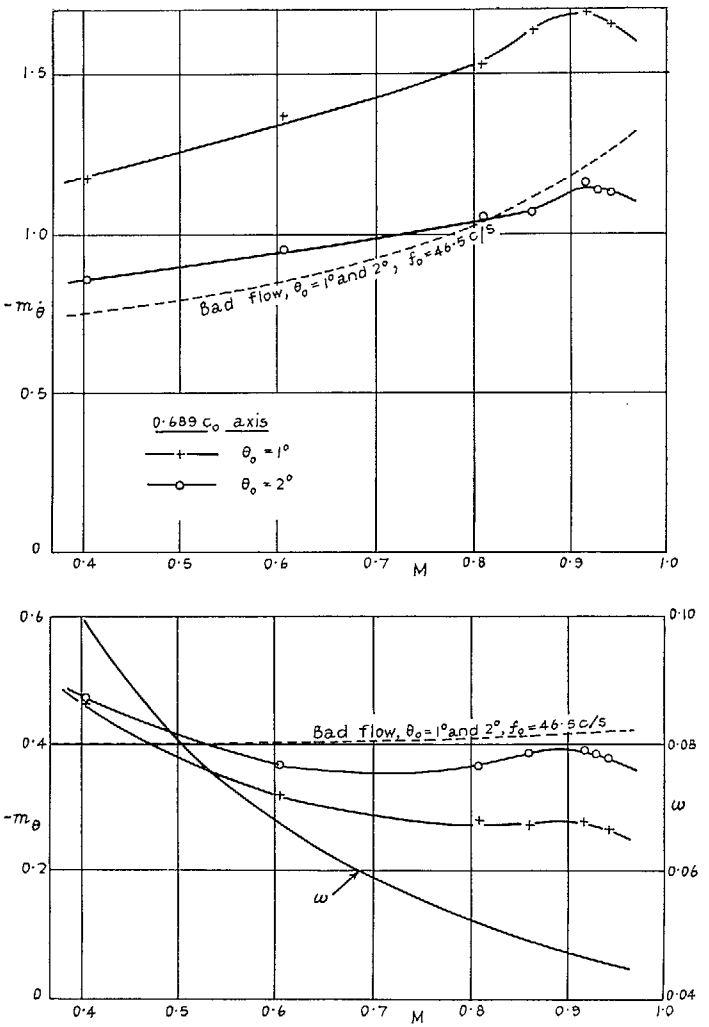

FIG. 22. Wing B—Values of $-m_{\dot{\theta}}$ and $-m_\theta$ for $\alpha = 0°$ and $f_0 = 35{\cdot}1$ c/s.

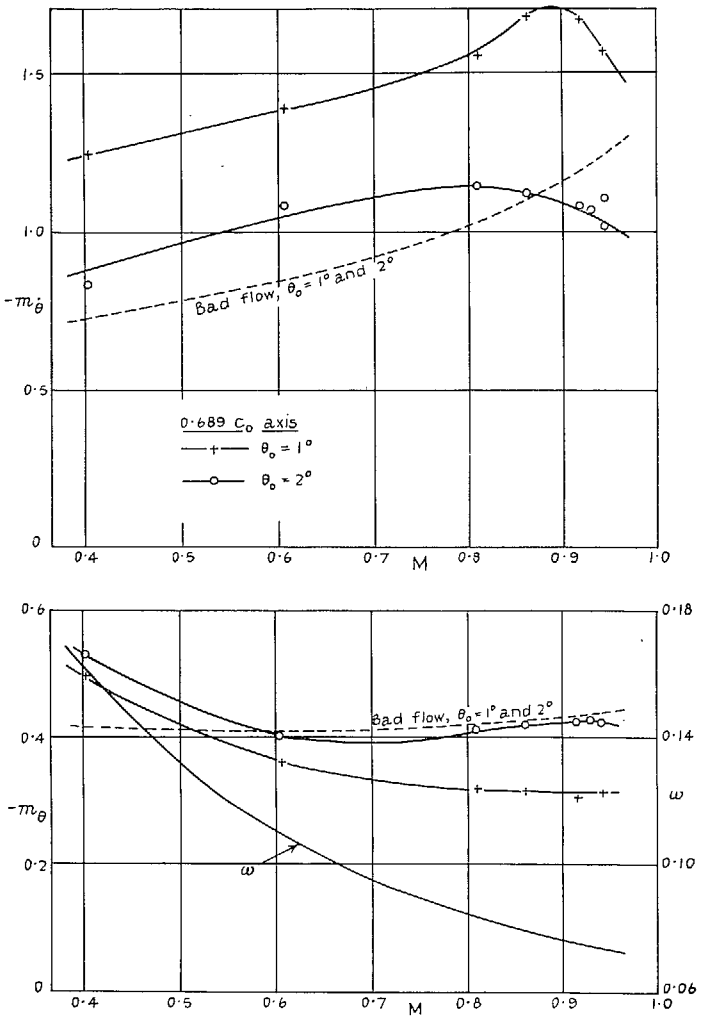

FIG. 23. Wing B—Values of $-m_{\dot\theta}$ and $-m_\theta$ for $\alpha = 0°$ and $f_0 = 56{\cdot}9$ c/s.

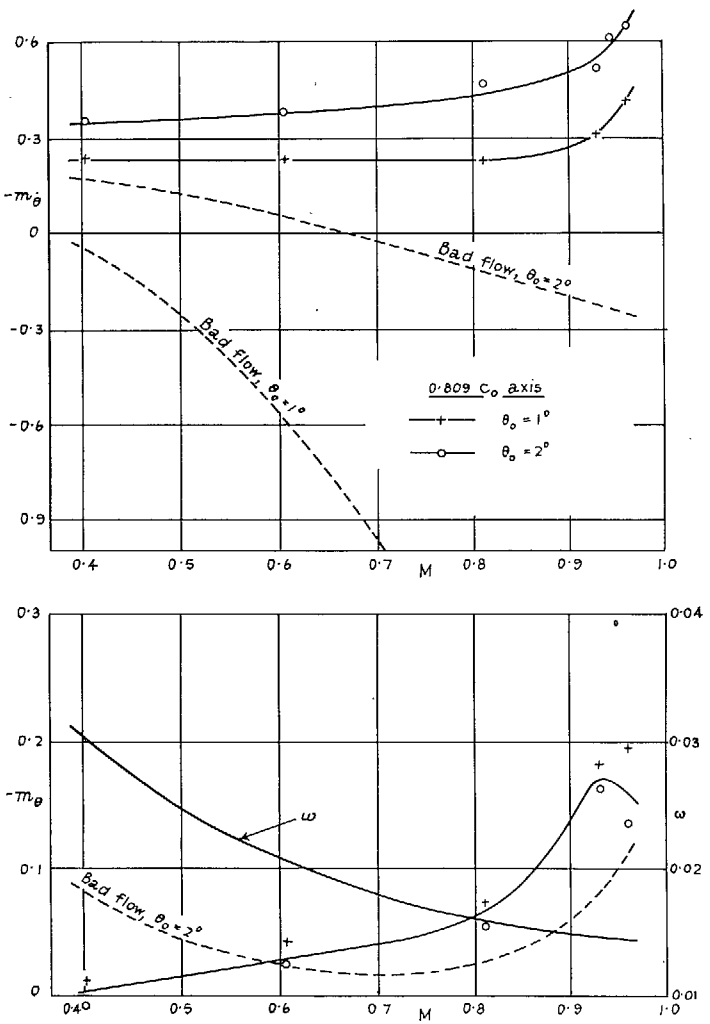

FIG. 24. Wing C—Values of $-m_{\dot\theta}$ and $-m_\theta$ for $\alpha = 0°$ and $f_0 = 11{\cdot}2$ c/s.

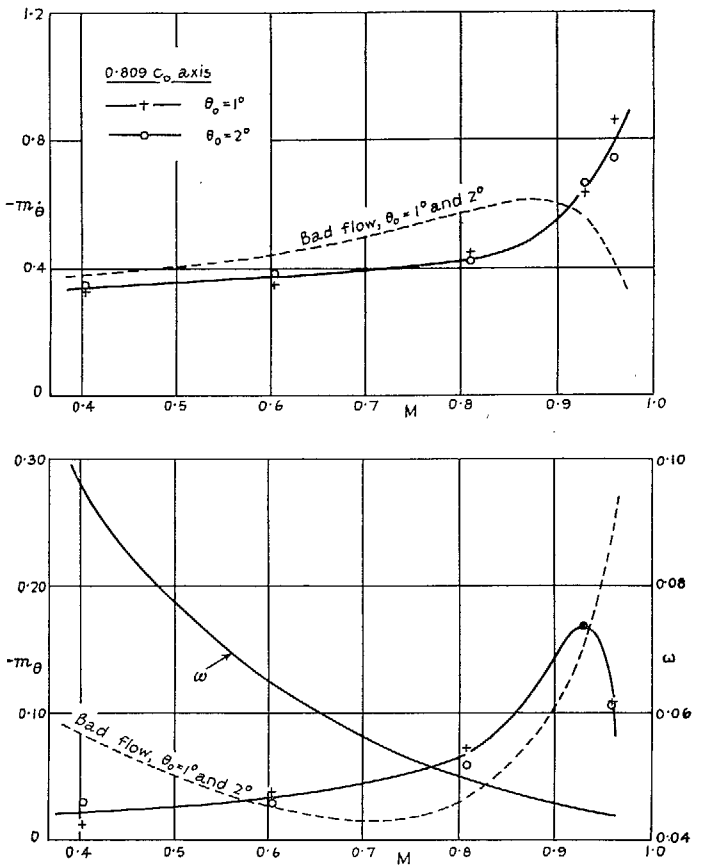

FIG. 25. Wing C—Values of $-m_{\dot\theta}$ and $-m_\theta$ for $\alpha = 0°$ and $f_0 = 35{\cdot}0$ c/s.

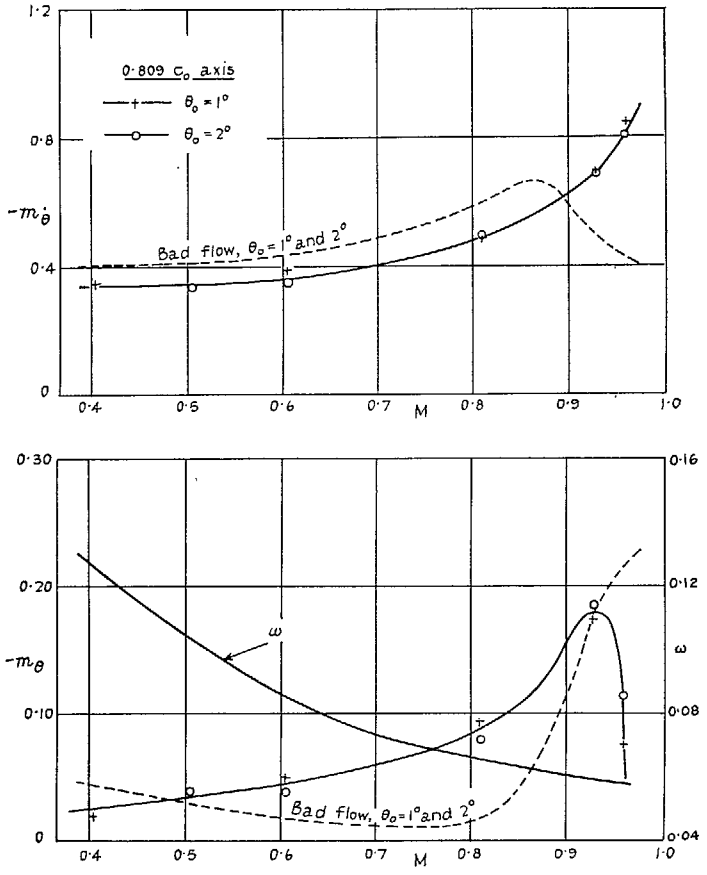

FIG. 26. Wing C—Values of $-m_{\dot\theta}$ and $-m_\theta$ for $\alpha = 0°$ and $f_0 = 46{\cdot}4$ c/s.

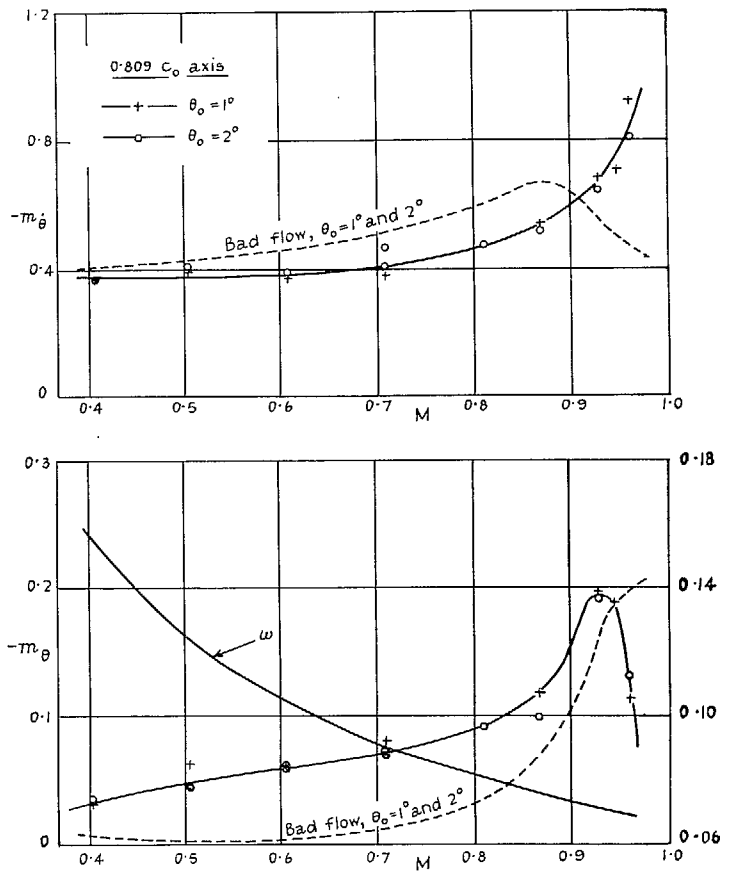

FIG. 27. Wing C—Values of $-m_{\dot\theta}$ and $-m_\theta$ for $\alpha = 0°$ and $f_0 = 56{\cdot}9$ c/s.

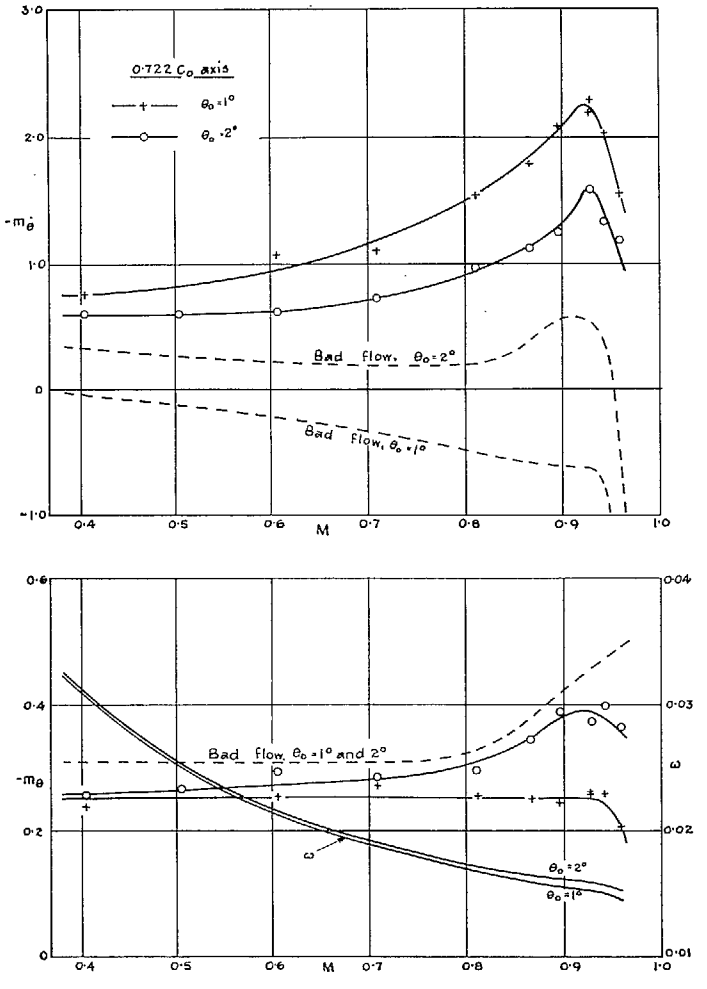

FIG. 28. Wing C—Values of $-m_{\dot\theta}$ and $-m_\theta$ for $\alpha = 0°$ and $f_0 = 11{\cdot}1$ c/s.

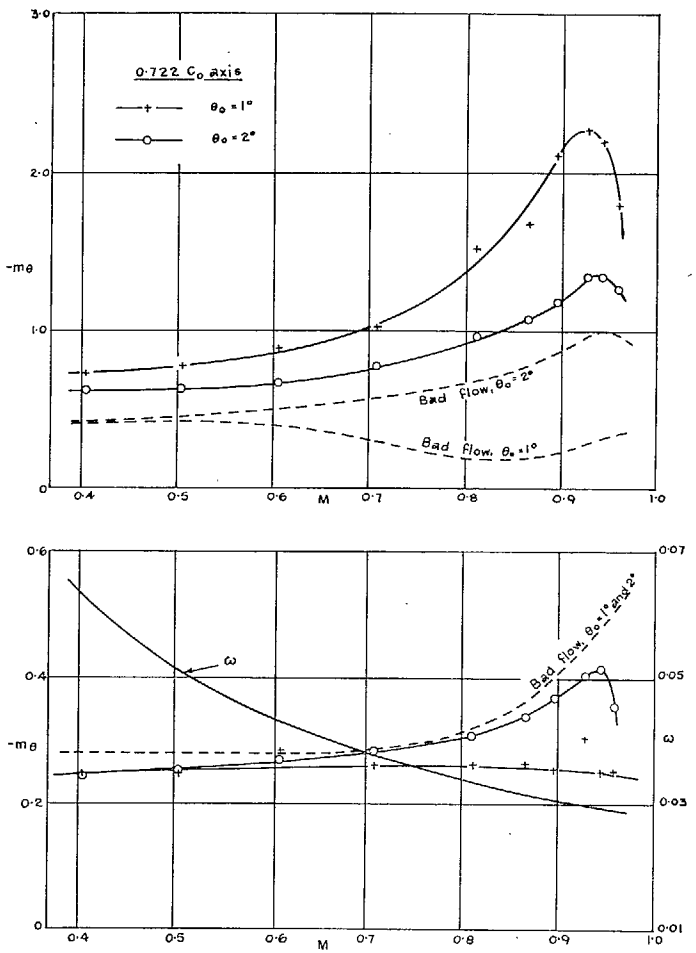

FIG. 29. Wing C—Values of $-m_j$ and $-m_\theta$ for $\alpha = 0°$ and $f_0 = 23{\cdot}3$ c/s.

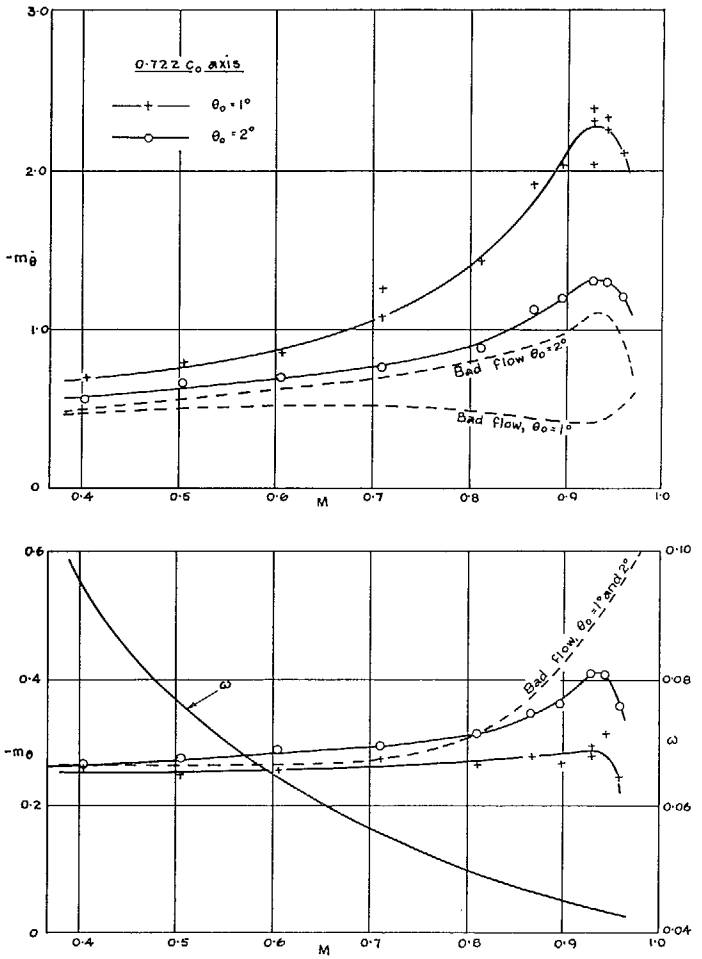

FIG. 30. Wing C—Values of $-m_{\dot\theta}$ and $-m_\theta$ for $\alpha = 0°$ and $f_0 = 35{\cdot}1$ c/s.

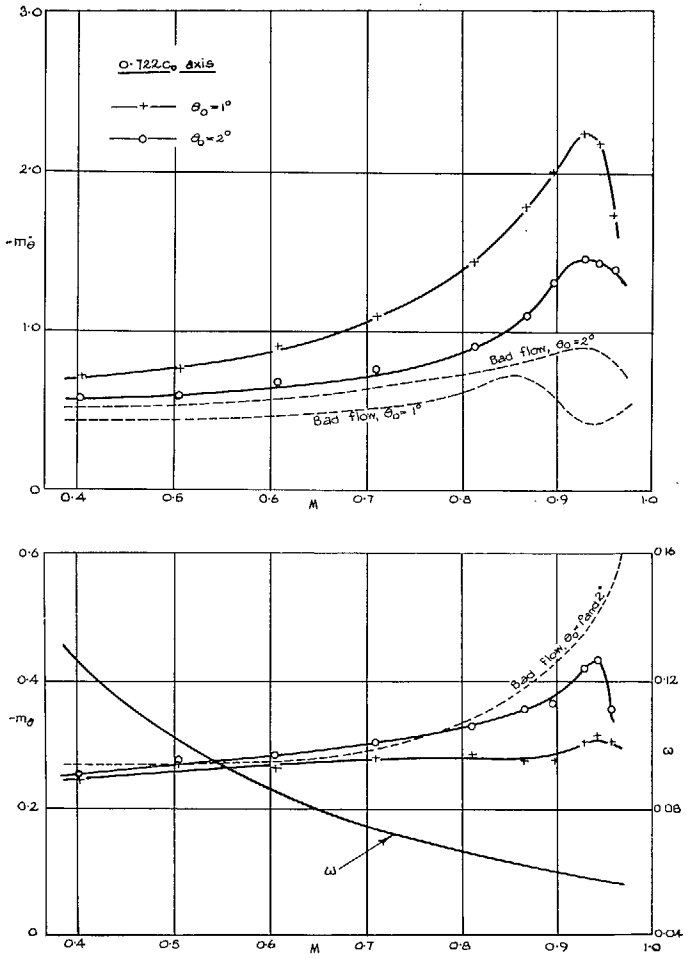

FIG. 31. Wing C—Values of $-m_{\dot\theta}$ and $-m_\theta$ for $\alpha = 0°$ and $f_0 = 46{\cdot}4$ c/s.

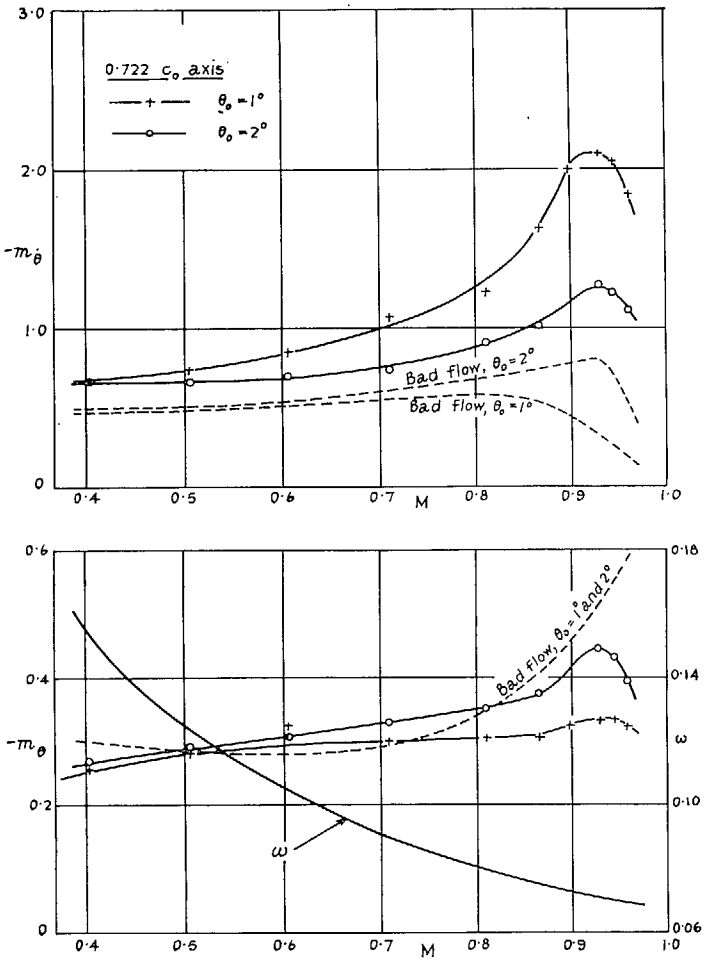

FIG. 32. Wing C—Values of $-m_{\dot\theta}$ and $-m_\theta$ for $\alpha = 0°$ and $f_0 = 56{\cdot}8$ c/s.

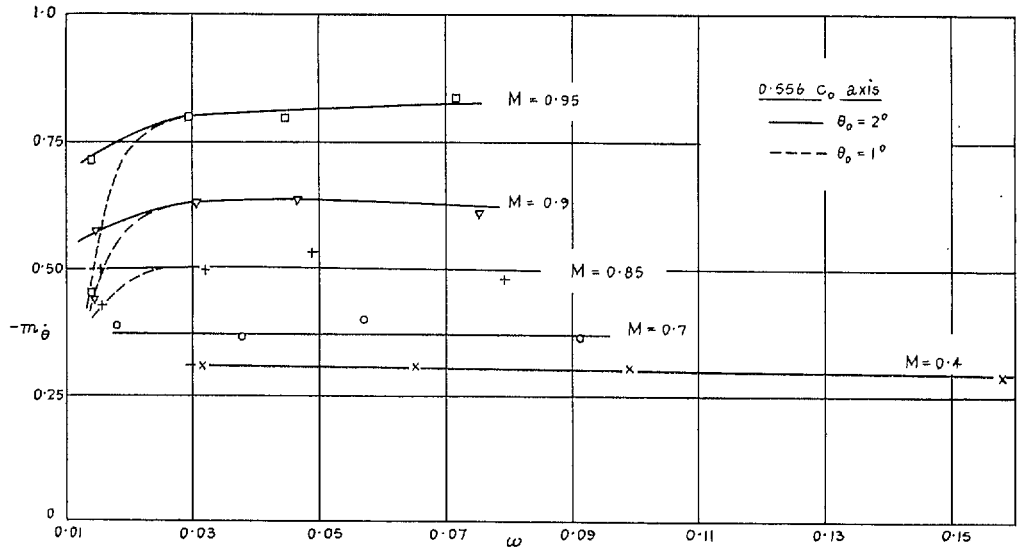

FIG. 33 Wing A—Dependence of $-m_{\dot{\theta}}$ on ω for $\alpha = 0°$.

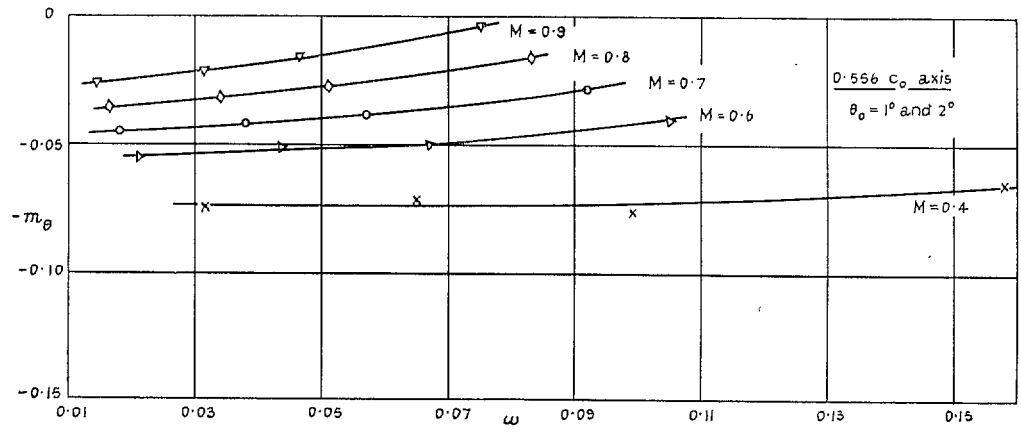

FIG. 34. Wing A—Dependence of $-m_{\theta}$ on ω for $\alpha = 0°$.

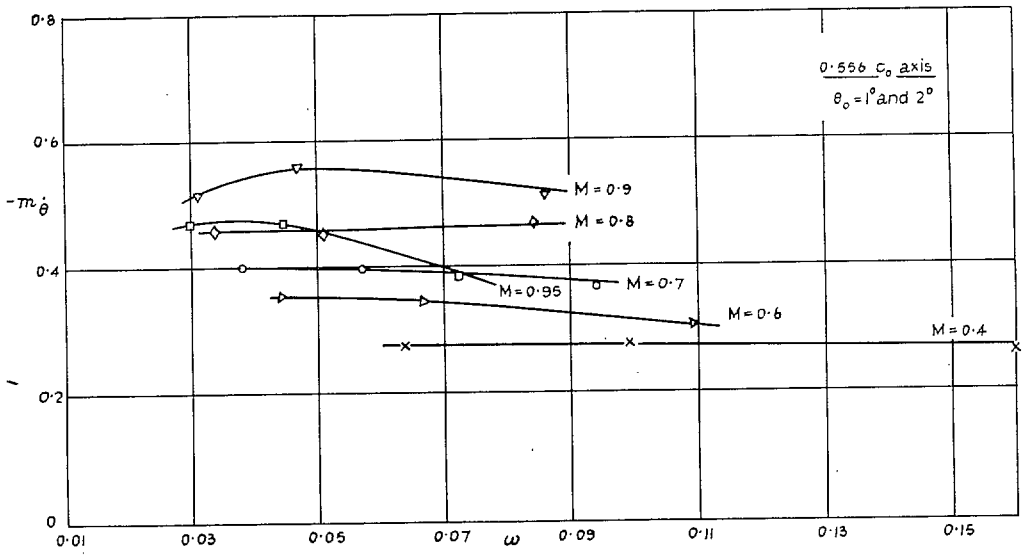

FIG. 35. Wing A—Dependence of $-m_{\dot{\theta}}$ on ω for $\alpha = 3°$.

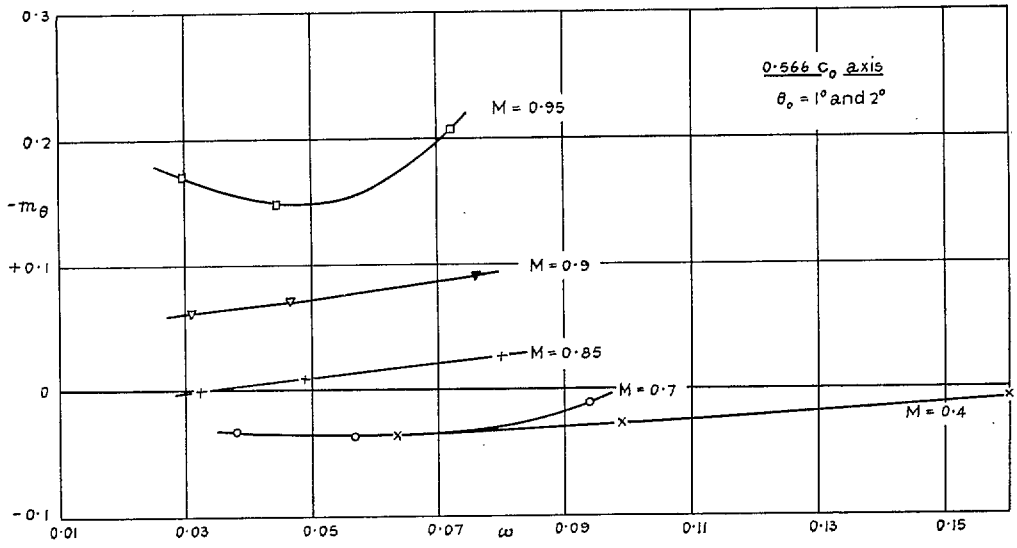

FIG. 36. Wing A—Dependence of $-m_{\theta}$ on ω for $\alpha = 3°$.

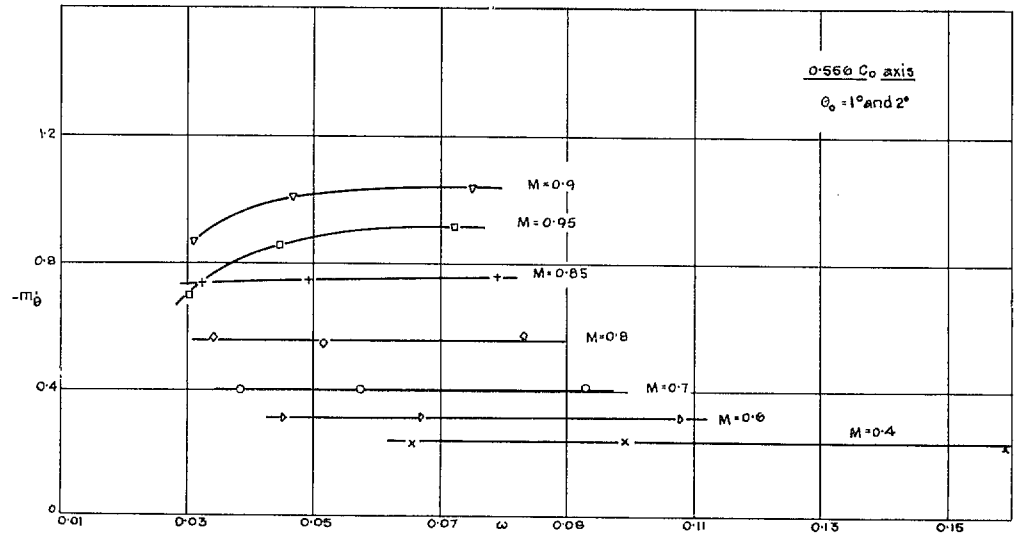

FIG. 37. Wing A—Dependence of $-m_{\dot{\theta}}$ on ω for $\alpha = 5°$.

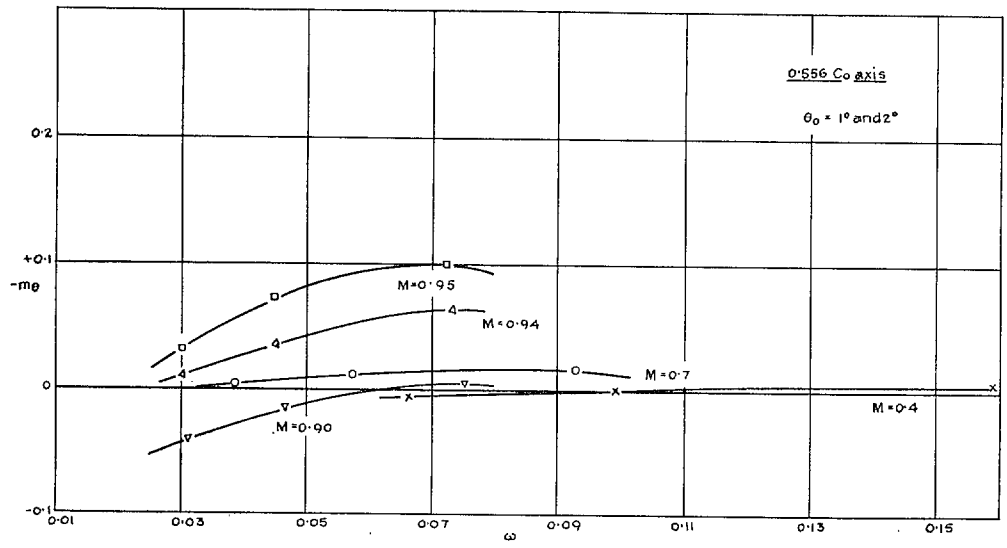

FIG. 38. Wing A—Dependence of $-m_{\theta}$ on ω for $\alpha = 5°$.

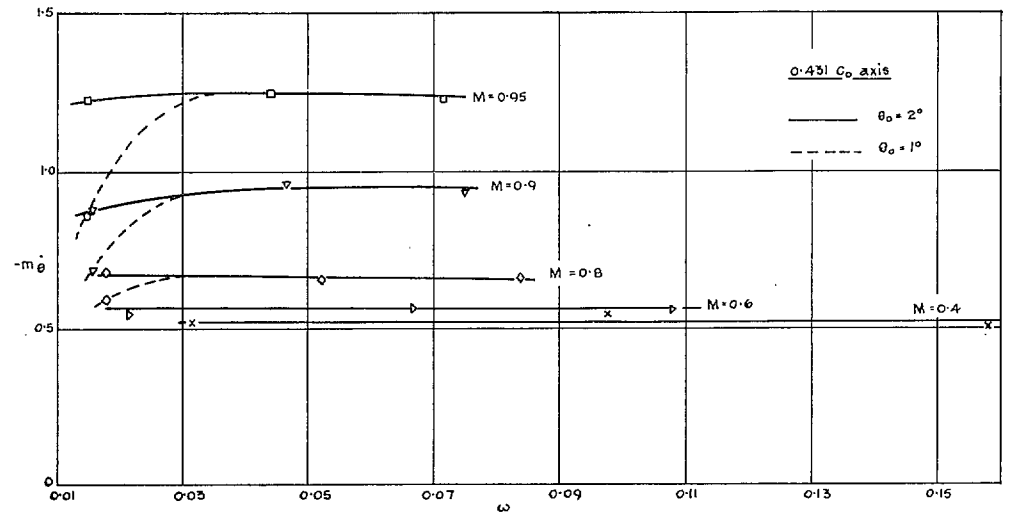

FIG. 39. Wing A—Dependence of $-m_{\dot{\theta}}$ on ω for $\alpha = 0°$.

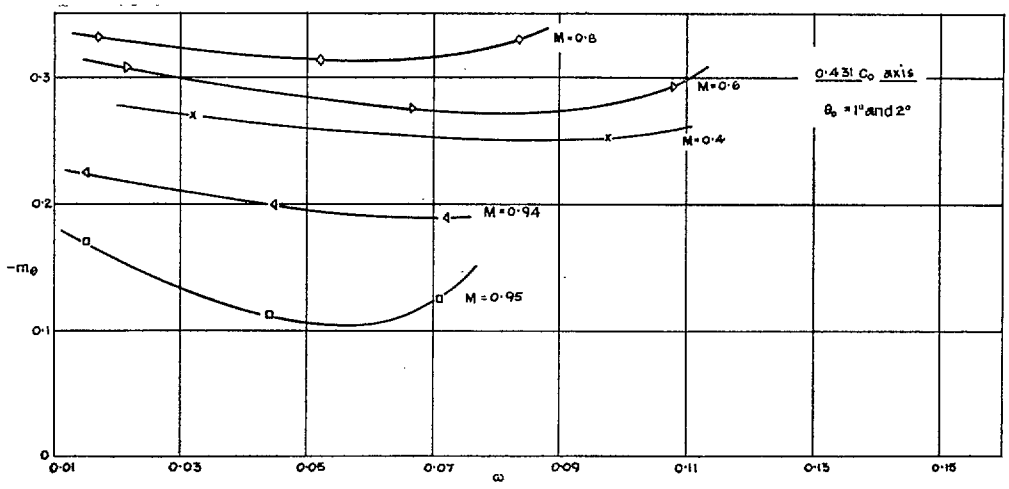

FIG. 40. Wing A—Dependence of $-m_{\theta}$ on ω for $\alpha = 0°$.

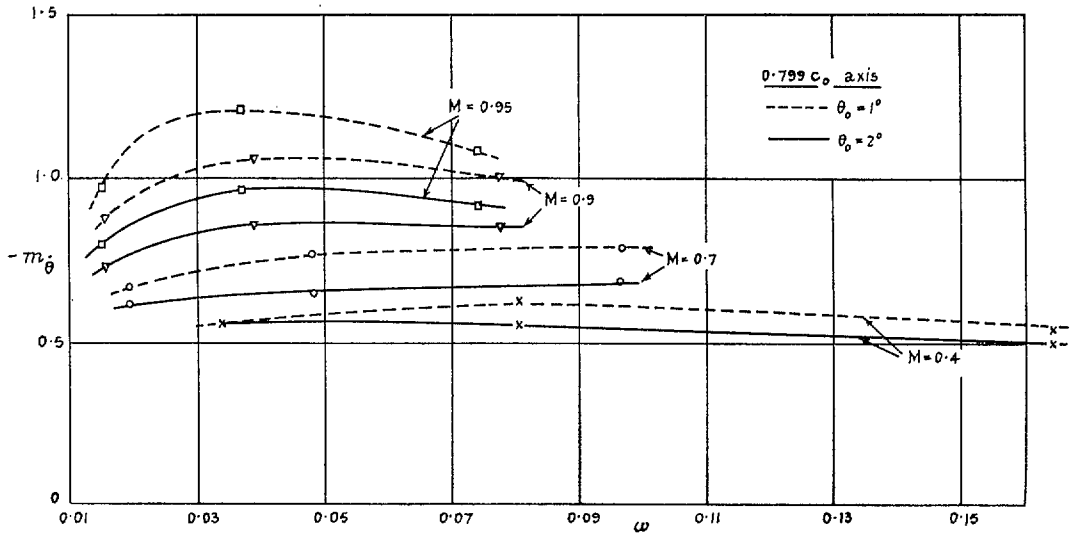

FIG. 41. Wing B—Dependence of $-m_{\dot{\theta}}$ on ω.

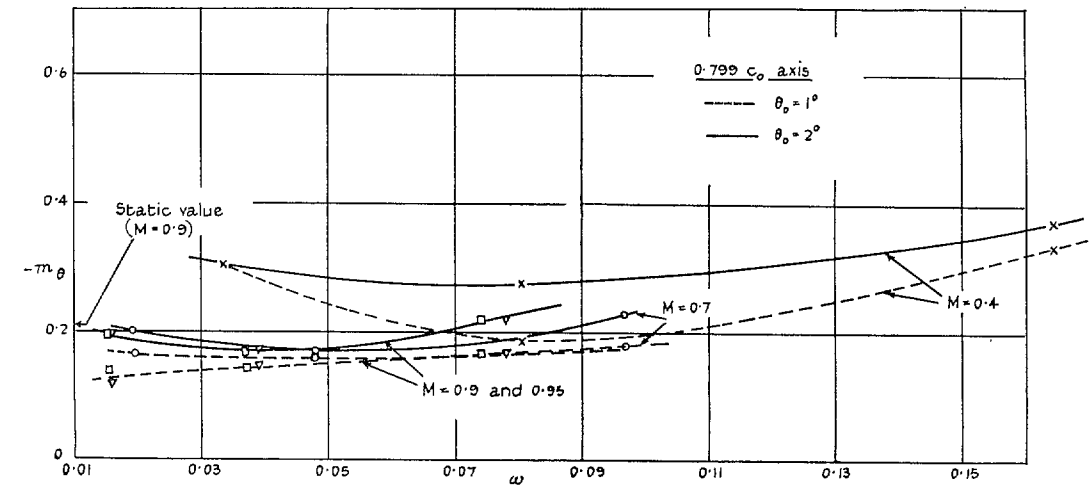

FIG. 42. Wing B—Dependence of $-m_{\theta}$ on ω.

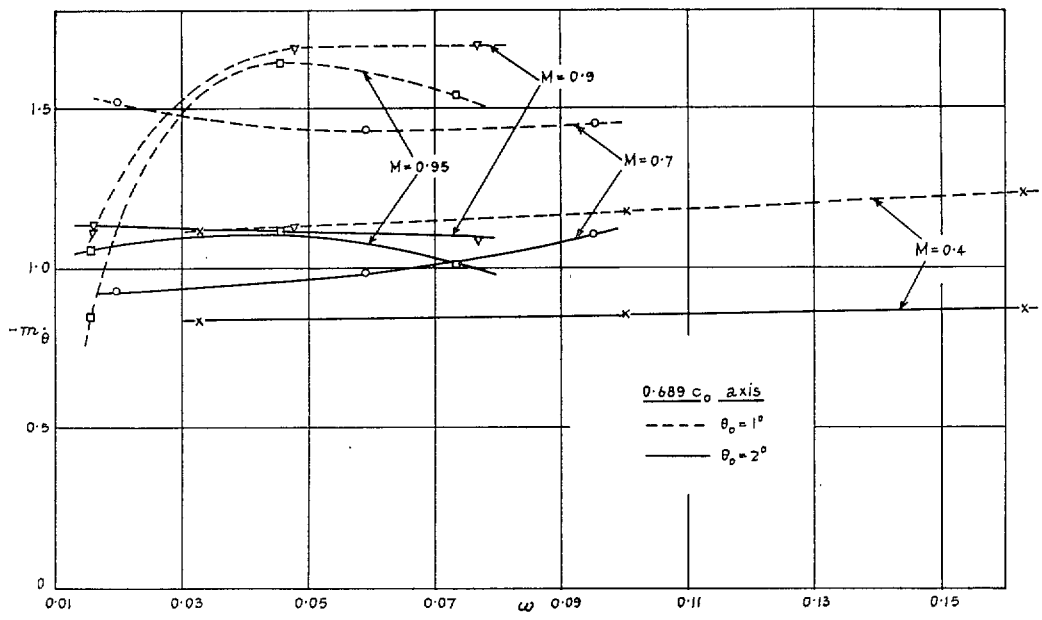

FIG. 43. Wing B—Dependence of $-m_{\dot{\theta}}$ on ω.

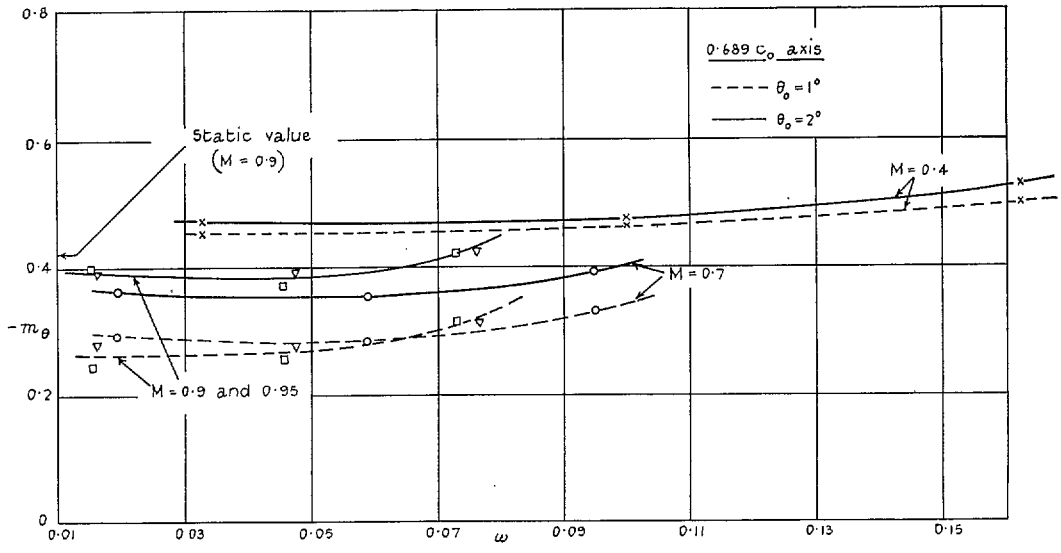

FIG. 44. Wing B—Dependence of $-m_{\theta}$ on ω.

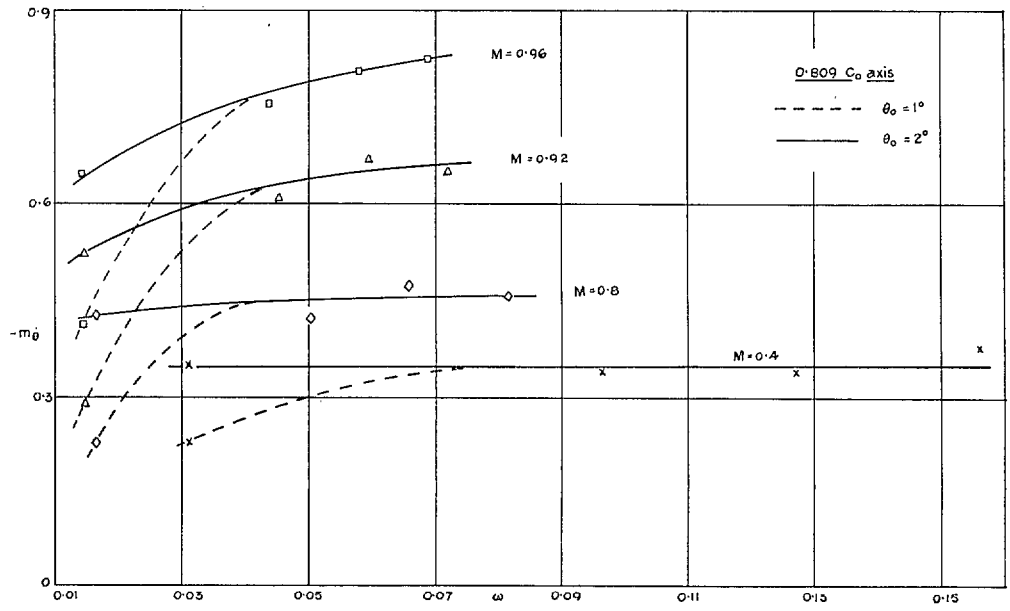

FIG. 45. Wing C—Dependence of $-m_{\dot\theta}$ on ω.

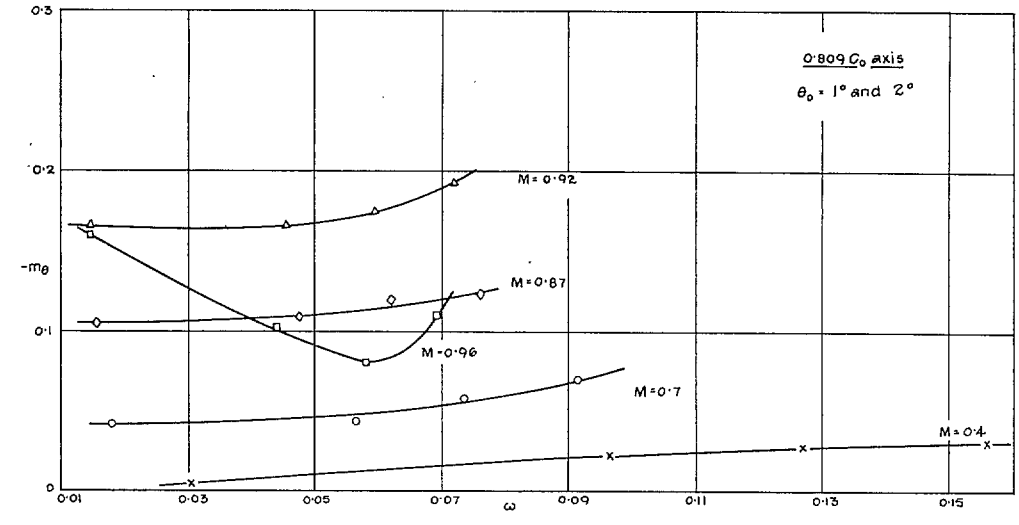

FIG. 46. Wing C—Dependence of $-m_{\dot\theta}$ on ω.

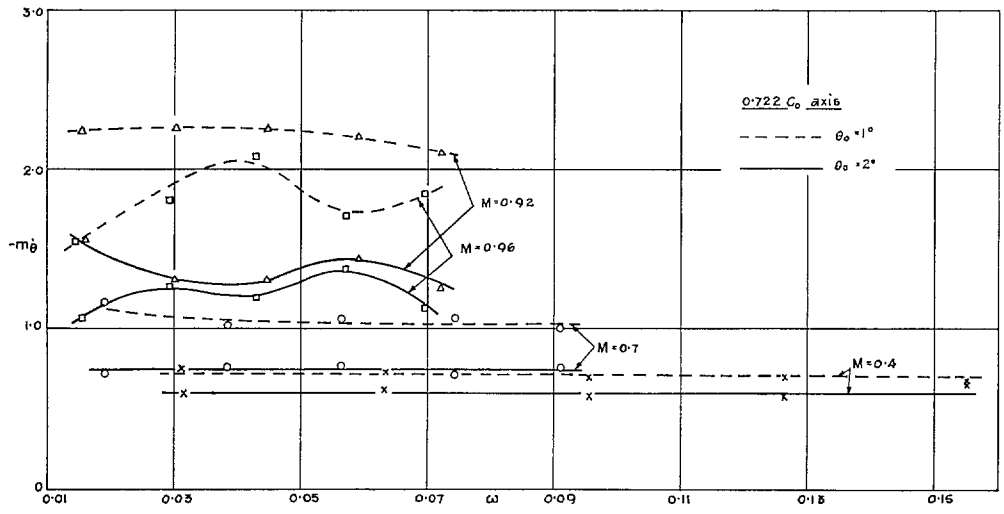

FIG. 47. Wing C—Dependence of $-m_{\dot{\theta}}$ on ω.

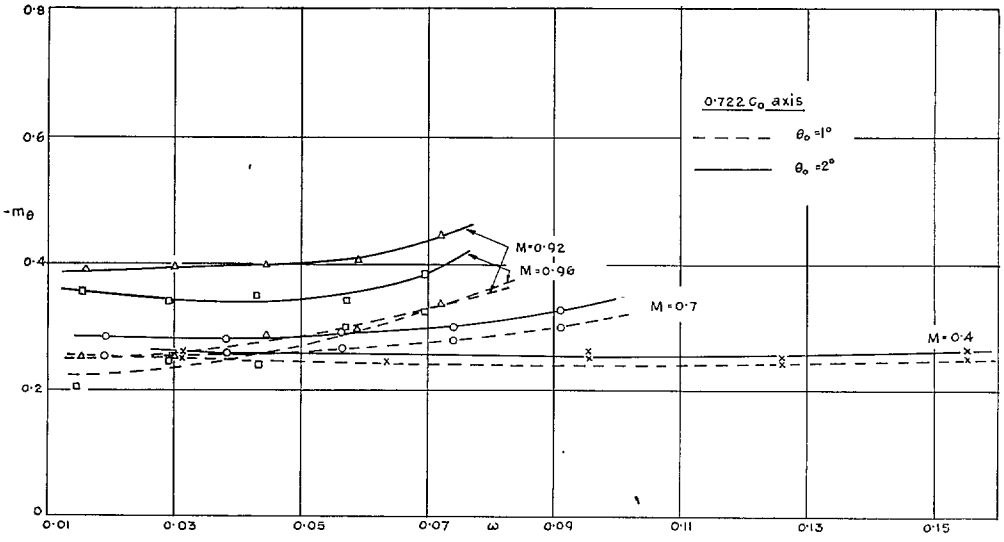

FIG. 48. Wing C—Dependence of $-m_{\theta}$ on ω.

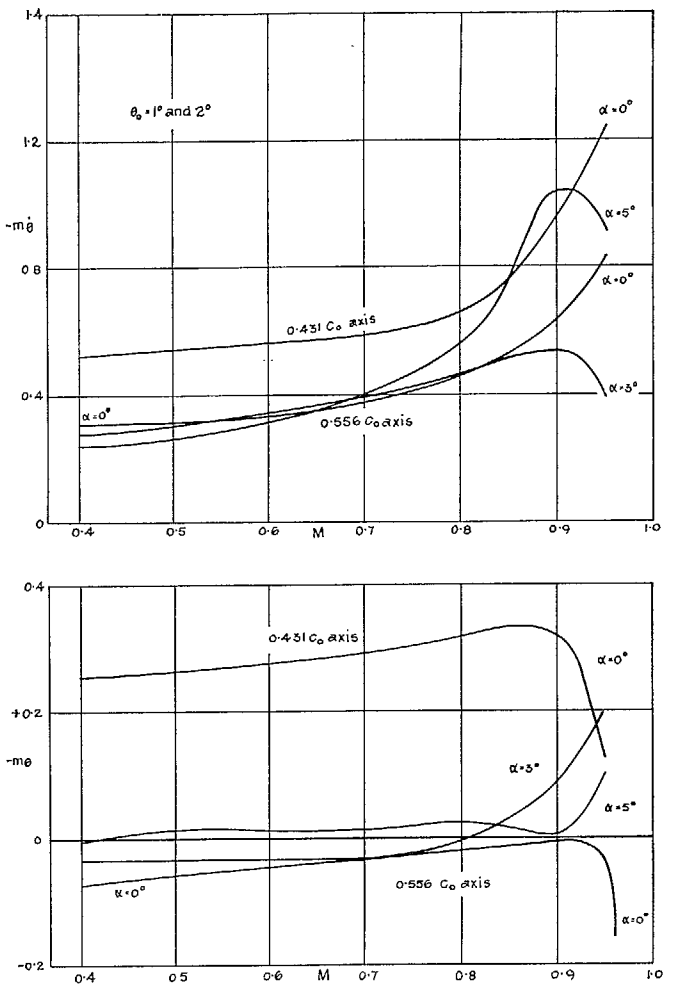

FIG. 49. Wing A—Dependence of $-m_{\dot\theta}$ and $-m_\theta$ on M for $\omega = 0{\cdot}07$.

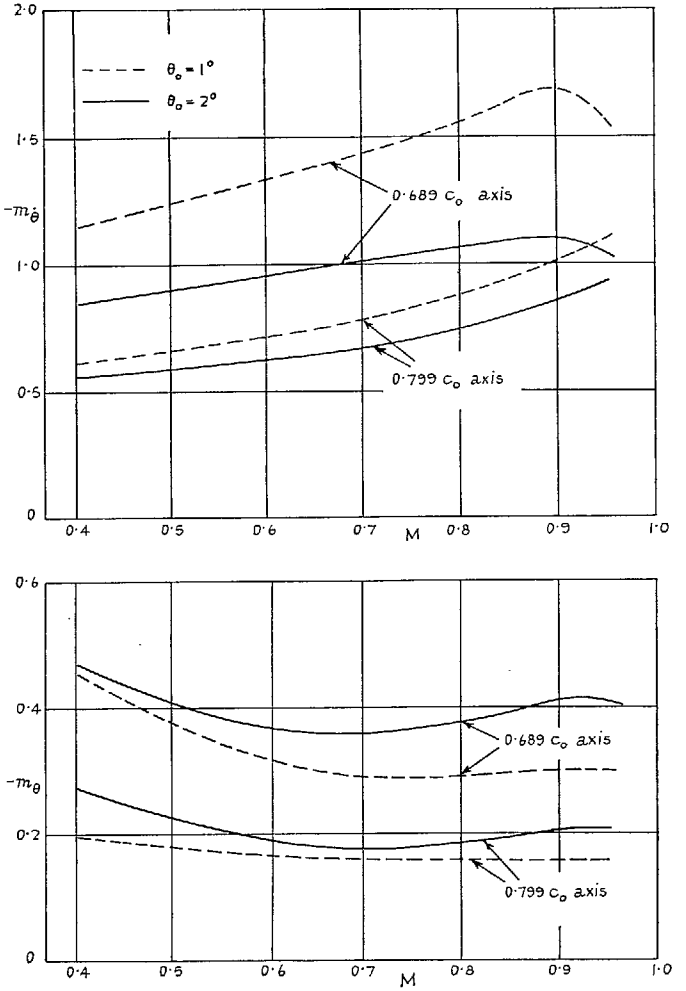

FIG. 50. Wing B—Dependence of $-m_{\dot\theta}$ and $-m_\theta$ on M for $\omega = 0{\cdot}07$.

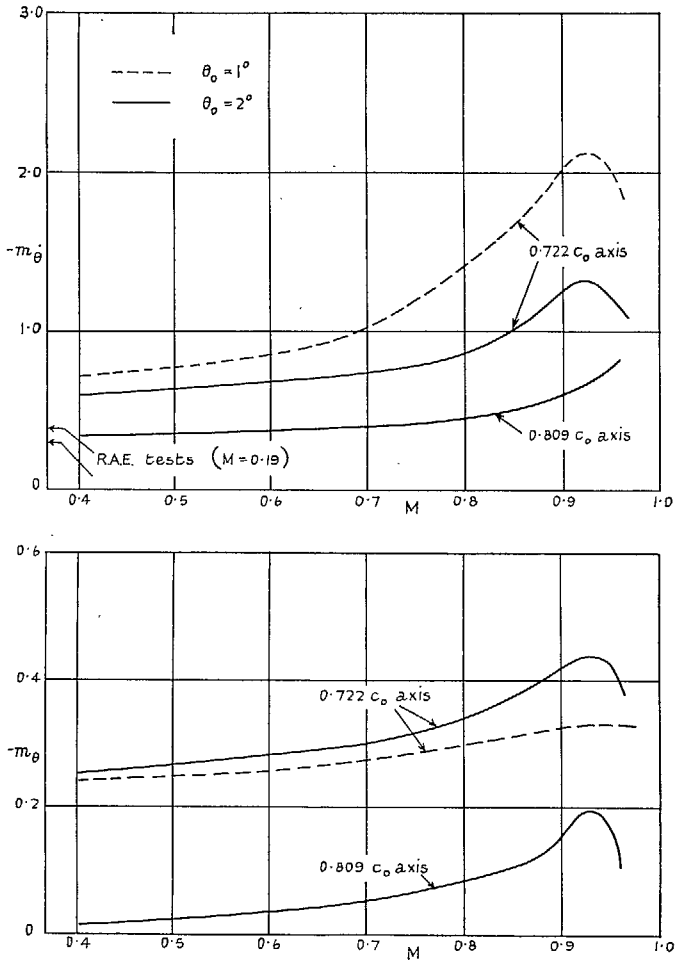

FIG. 51. Wing C—Dependence of $-m_{\dot\theta}$ and $-m_\theta$ on M for $\omega = 0{\cdot}07$.

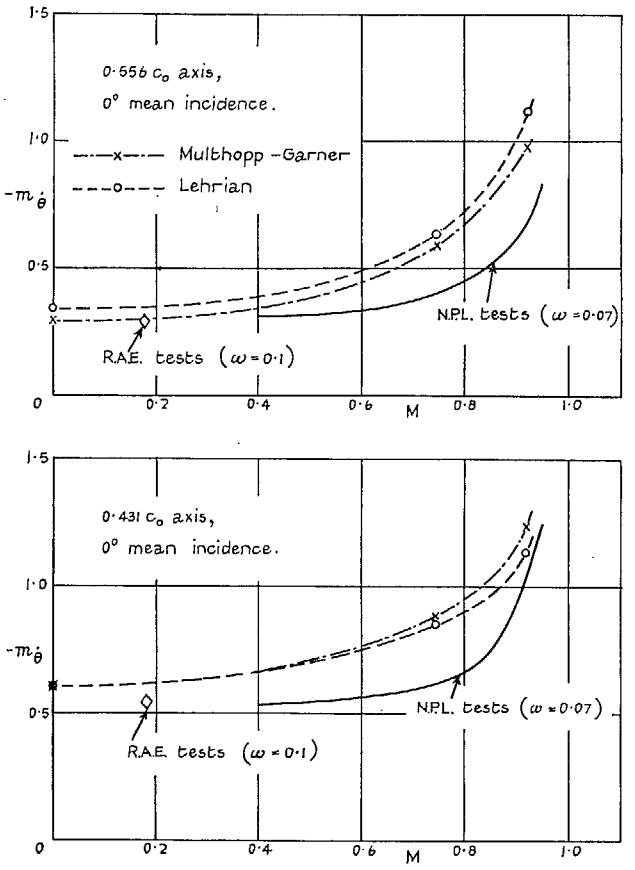

FIG. 52. Comparison with theory and R.A.E. tests for Wing A.

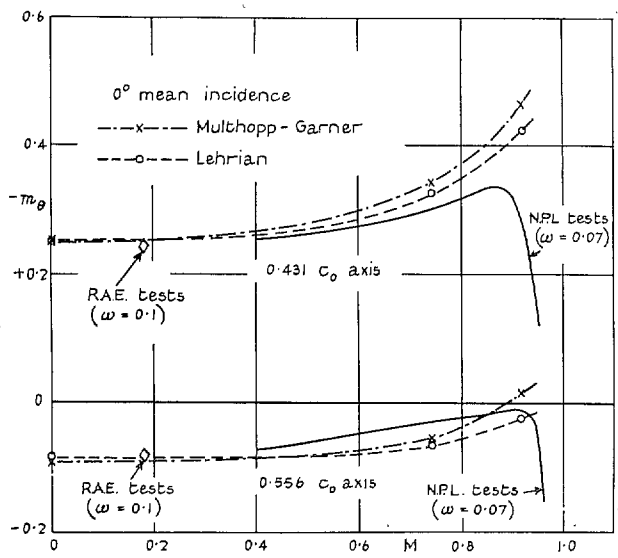

FIG. 53. Comparison with theory and R.A.E. tests for Wing A.

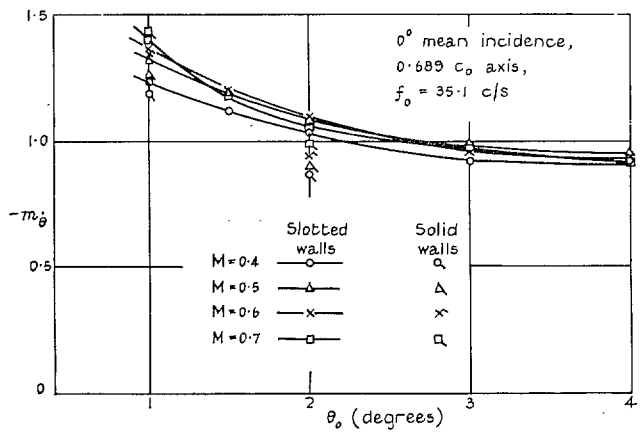

FIG. 54. Amplitude effects with Wing B.

(92036) Wt. 67/7689 K5 9/65 Hw.

Publications of the Aeronautical Research Council

ANNUAL TECHNICAL REPORTS OF THE AERONAUTICAL RESEARCH COUNCIL (BOUND VOLUMES)

1945 Vol. I. Aero and Hydrodynamics, Aerofoils. £6 10s. (£6 14s.)
Vol. II. Aircraft, Airscrews, Controls. £6 10s. (£6 14s.)
Vol. III. Flutter and Vibration, Instruments, Miscellaneous, Parachutes, Plates and Panels, Propulsion. £6 10s. (£6 14s.)
Vol. IV. Stability, Structures, Wind Tunnels, Wind Tunnel Technique. £6 10s. (£6 14s.)

1946 Vol. I. Accidents, Aerodynamics, Aerofoils and Hydrofoils. £8 8s. (£8 12s. 6d.)
Vol. II. Airscrews, Cabin Cooling, Chemical Hazards, Controls, Flames, Flutter, Helicopters, Instruments and Instrumentation, Interference, Jets, Miscellaneous, Parachutes. £8 8s. (£8 12s.)
Vol. III. Performance, Propulsion, Seaplanes, Stability, Structures, Wind Tunnels. £8 8s. (£8 12s.)

1947 Vol. I. Aerodynamics, Aerofoils, Aircraft. £8 8s. (£8 12s. 6d.)
Vol. II. Airscrews and Rotors, Controls, Flutter, Materials, Miscellaneous, Parachutes, Propulsion, Seaplanes, Stability, Structures, Take-off and Landing. £8 8s. (£8 12s. 6d.)

1948 Vol. I. Aerodynamics, Aerofoils, Aircraft, Airscrews, Controls, Flutter and Vibration, Helicopters, Instruments, Propulsion, Seaplane, Stability, Structures, Wind Tunnels. £6 10s. (£6 14s.)
Vol. II. Aerodynamics, Aerofoils, Aircraft, Airscrews, Controls, Flutter and Vibration, Helicopters, Instruments, Propulsion, Seaplane, Stability, Structures, Wind Tunnels. £5 10s. (£5 14s.)

1949 Vol. I. Aerodynamics, Aerofoils. £5 10s. (£5 14s.)
Vol. II. Aircraft, Controls, Flutter and Vibration, Helicopters, Instruments, Materials, Seaplanes, Structures, Wind Tunnels. £5 10s. (£5 13s. 6d.)

1950 Vol. I. Aerodynamics, Aerofoils, Aircraft. £5 12s. 6d. (£5 16s. 6d.)
Vol. II. Apparatus, Flutter and Vibration, Meteorology, Panels, Performance, Rotorcraft, Seaplanes. £4 (£4 3s. 6d.)
Vol. III. Stability and Control, Structures, Thermodynamics, Visual Aids, Wind Tunnels. £4 (£4 3s. 6d.)

1951 Vol. I. Aerodynamics, Aerofoils. £6 10s. (£6 14s.)
Vol. II. Compressors and Turbines, Flutter, Instruments, Mathematics, Ropes, Rotorcraft, Stability and Control, Structures, Wind Tunnels. £5 10s. (£5 14s.)

1952 Vol. I. Aerodynamics, Aerofoils. £8 8s. (£8 12s.)
Vol. II. Aircraft, Bodies, Compressors, Controls, Equipment, Flutter and Oscillation, Rotorcraft, Seaplanes, Structures. £5 10s. (£5 13s. 6d.)

1953 Vol. I. Aerodynamics, Aerofoils and Wings, Aircraft, Compressors and Turbines, Controls. £6 (£6 4s.)
Vol. II. Flutter and Oscillation, Gusts, Helicopters, Performance, Seaplanes, Stability, Structures, Thermodynamics, Turbulence. £5 5s. (£5 9s.)

1954 Aero and Hydrodynamics, Aerofoils, Arrester gear, Compressors and Turbines, Flutter, Materials, Performance, Rotorcraft, Stability and Control, Structures. £7 7s. (£7 11s.)

Special Volumes

Vol. I. Aero and Hydrodynamics, Aerofoils, Controls, Flutter, Kites, Parachutes, Performance, Propulsion, Stability. £6 6s. (£6 9s. 6d.)
Vol. II. Aero and Hydrodynamics, Aerofoils, Airscrews, Controls, Flutter, Materials, Miscellaneous, Parachutes, Propulsion, Stability, Structures. £7 7s. (£7 10s. 6d.)
Vol. III. Aero and Hydrodynamics, Aerofoils, Airscrews, Controls, Flutter, Kites, Miscellaneous, Parachutes, Propulsion, Seaplanes, Stability, Structures, Test Equipment. £9 9s. (£9 13s. 6d.)

Reviews of the Aeronautical Research Council

1949–54 5s. (5s. 6d.)

Index to all Reports and Memoranda published in the Annual Technical Reports

1909–1947 R. & M. 2600 (out of print)

Indexes to the Reports and Memoranda of the Aeronautical Research Council

Between Nos. 2451–2549: R. & M. No. 2550 2s. 6d. (2s. 9d.); Between Nos. 2651–2749: R. & M. No. 2750 2s. 6d. (2s. 9d.); Between Nos. 2751–2849: R. & M. No. 2850 2s. 6d. (2s. 9d.); Between Nos. 2851–2949: R. & M. No. 2950 3s. (3s. 3d.); Between Nos. 2951–3049: R. & M. No. 3050 3s. 6d. (3s. 9d.); Between Nos. 3051–3149: R. & M. No. 3150 3s. 6d. (3s. 9d.); Between Nos. 3151–3249: R. & M. No. 3250 3s. 6d. (3s. 9d.); Between Nos. 3251–3349: R. & M. No. 3350 3s. 6d. (3s. 11d.)

Prices in brackets include postage

Government publications can be purchased over the counter or by post from the Government Bookshops in London, Edinburgh, Cardiff, Belfast, Manchester, Birmingham and Bristol, or through any bookseller

Printed and published by
HER MAJESTY'S STATIONERY OFFICE

To be purchased from
York House, Kingsway, London W.C.2
423 Oxford Street, London W.1
13A Castle Street, Edinburgh 2
109 St. Mary Street, Cardiff
39 King Street, Manchester 2
50 Fairfax Street, Bristol 1
35 Smallbrook, Ringway, Birmingham 5
80 Chichester Street, Belfast 1
or through any bookseller

Printed in England

S.O. Code No. 23-3419